Electronic Supplementary Information

Effects of the rigid and sterically bulky structure of non-fused nonfullerene acceptors on transient photon-to-current dynamics

Seihou Jinnai,[a] Kasumi Murayama,[b] Keisuke Nagai,[a] Megumi Mineshita,[c] Kosaku Kato,[d] Azusa Muraoka,[c] Akira Yamakata,[d] Akinori Saeki,[e,f] Yasuhiro Kobori,[b,g] and Yutaka Ie[a,f]

[a] *The Institute of Scientific and Industrial Research (SANKEN), Osaka University, 8-1 Mihogaoka, Ibaraki, Osaka 567-0047, Japan.*
[b] *Department of Chemistry, Graduate School of Science, Kobe University, 1-1 Rokkodai-cho, Nada-ku, Kobe 657-8501, Japan.*
[c] *Department of Mathematics, Physics and Computer Science, Japan Women's University, 2-8-1, Mejirodai, Bunkyo-ku, Tokyo 112-8681, Japan.*
[d] *Graduate School of Natural Science & Technology, Okayama University, 3-1-1 Tsushima-naka, Okayama 700-8530, Japan.*
[e] *Department of Applied Chemistry, Graduate School of Engineering, Osaka University, 2-1 Yamadaoka, Suita, Osaka 565-0871, Japan.*
[f] *Innovative Catalysis Science Division, Institute for Open and Transdisciplinary Research Initiatives (OTRI), Osaka University, 2-1 Yamadaoka, Suita, Osaka 565-0871, Japan.*
[g] *Molecular Photoscience Research Center, Kobe University, 1-1 Rokkodai-cho, Nada-ku, Kobe 657-8501, Japan.*

Table of Contents

Schemes, Figures, and Tables

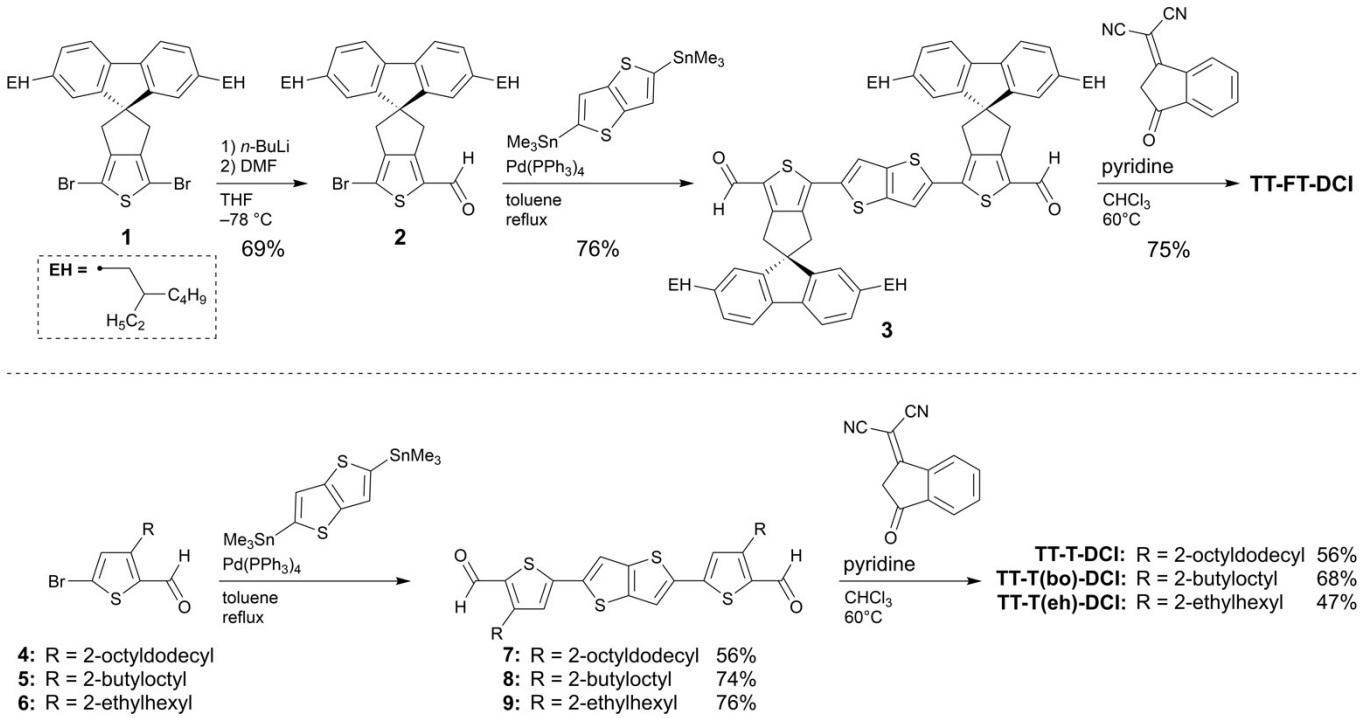

Scheme S1 Synthesis of acceptors.

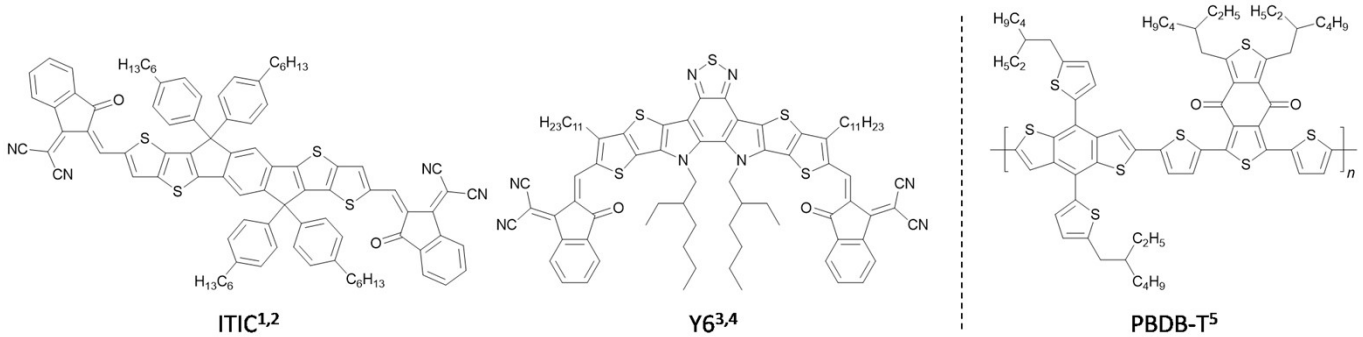

Fig. S1 Chemical structures for representative acceptors ITIC, Y6, and a donor PBDB-T.

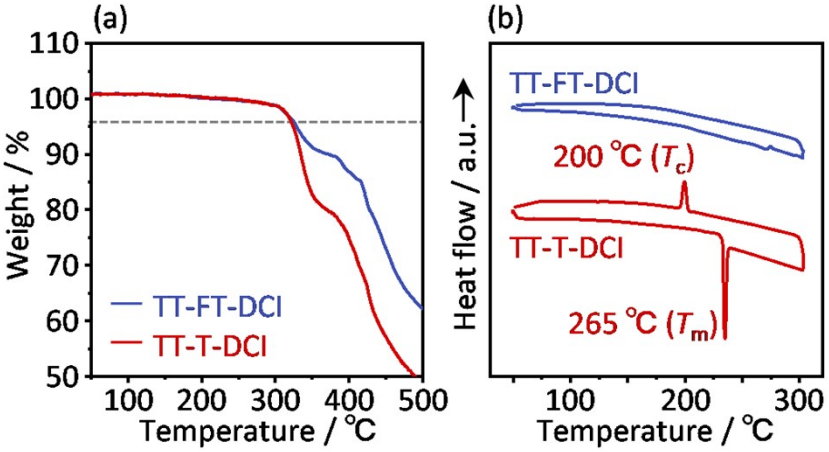

Fig. S2 (a) TGA and (b) DSC curves of TT-FT-DCI (blue) and TT-T-DCI (red) with a scanning rate of 10 °C min^{-1} under N_2.

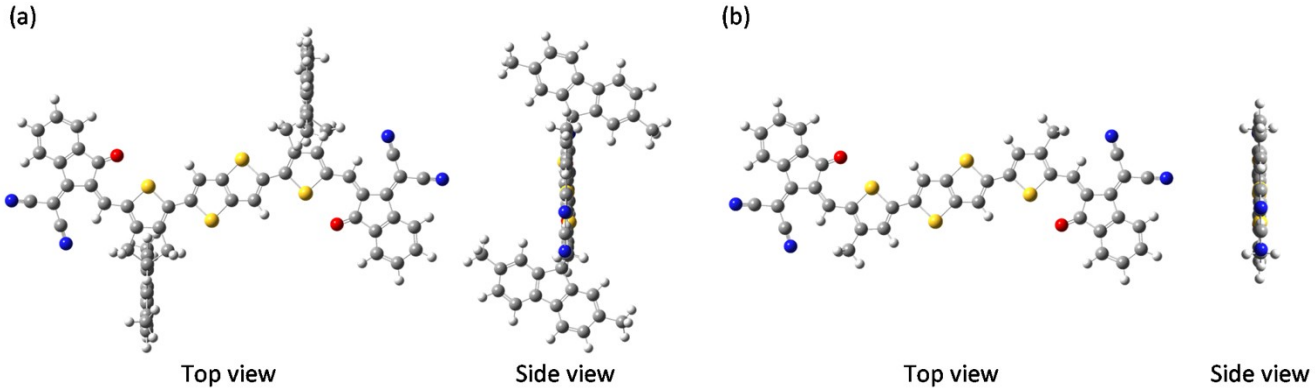

Fig. S3 Optimized structures of (a) TT-FT(m)-DCI and (b) TT-T(m)-DCI.

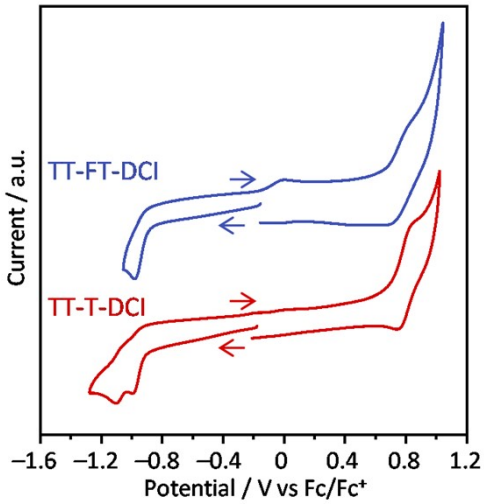

Fig. S4 Cyclic voltammograms of TT-FT-DCI and TT-T-DCI in CH_2Cl_2 containing 0.1 M $TBAPF_6$.

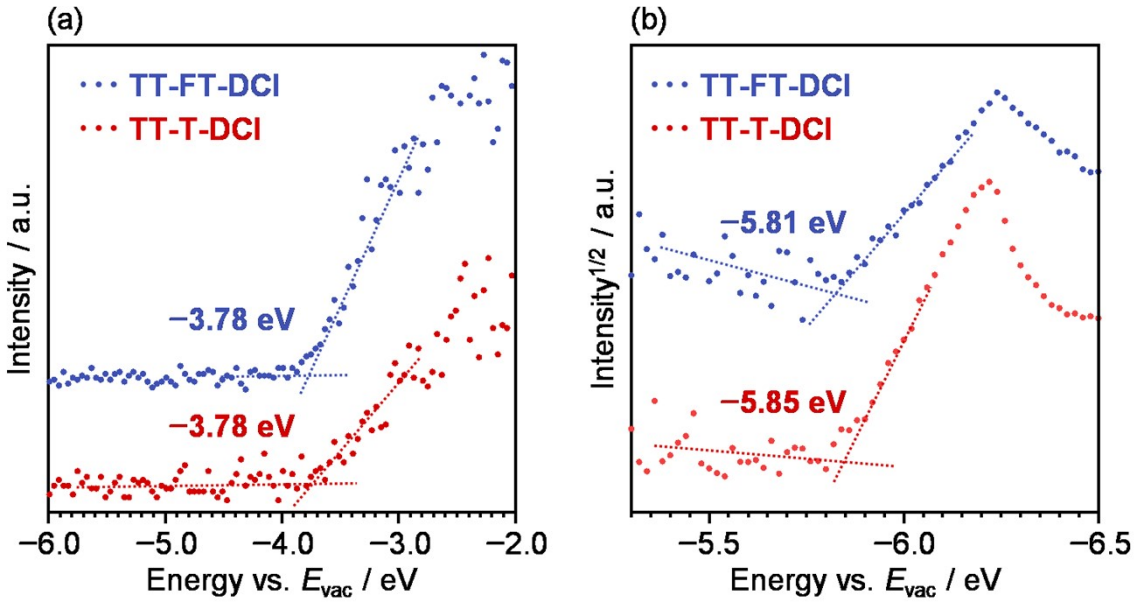

Fig. S5 (a) LEIPS and (b) PYS of TT-FT-DCI and TT-T-DCI in thin films.

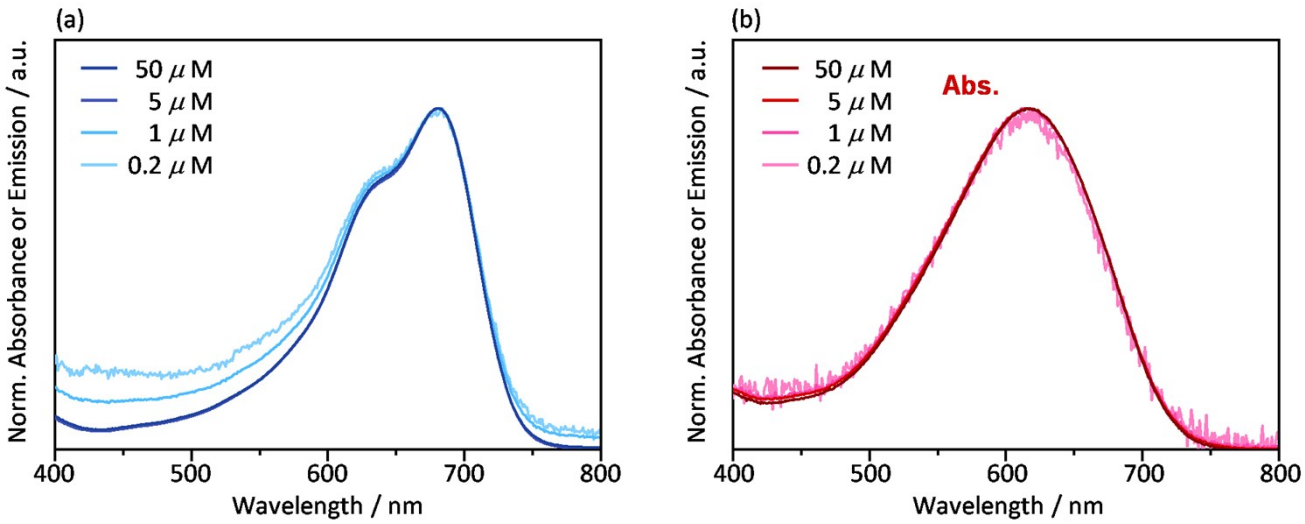

Fig. S6 Concentration-dependent UV-vis absorption spectra for (a) TT-FT-DCI and (b) TT-T-DCI in $CHCl_3$ solutions.

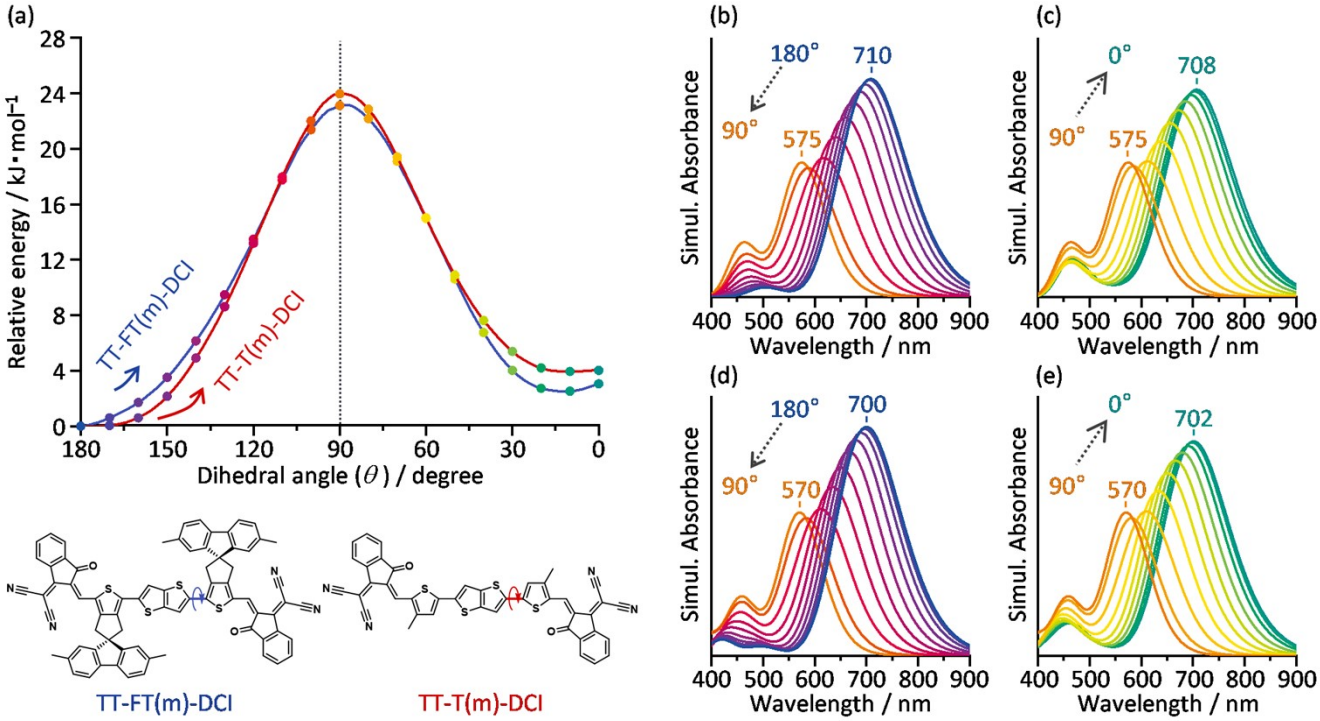

Fig. S7 (a) Potential energies against dihedral angles for TT-FT(m)-DCI and TT-T(m)-DCI, and (b) simulated absorption spectra for each optimized model compounds with dihedral angle (θ) fixed by every 10 degrees.

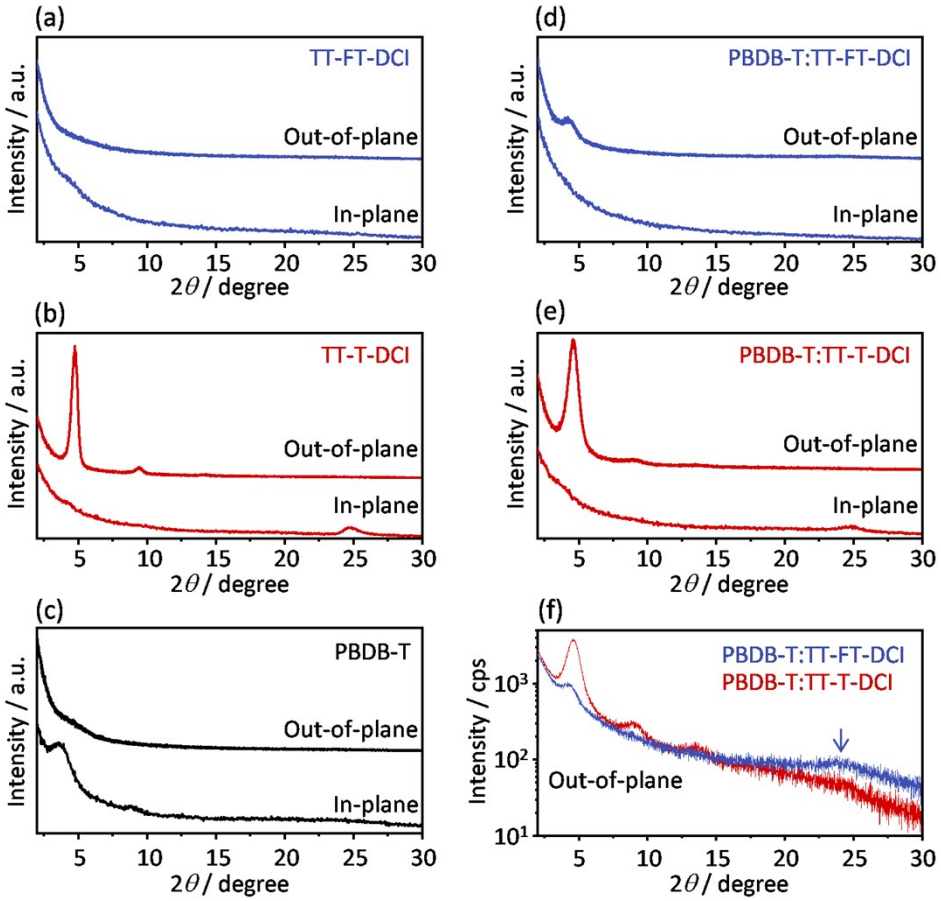

Fig. S8 X-ray diffractograms of pristine films (a, b, and c) and blend films (d, e, and f). The peak of $2\theta =$ 24° (blue arrow) in PBDB-T:TT-FT-DCI blend film in (f) indicates the face-on π-π stacking.

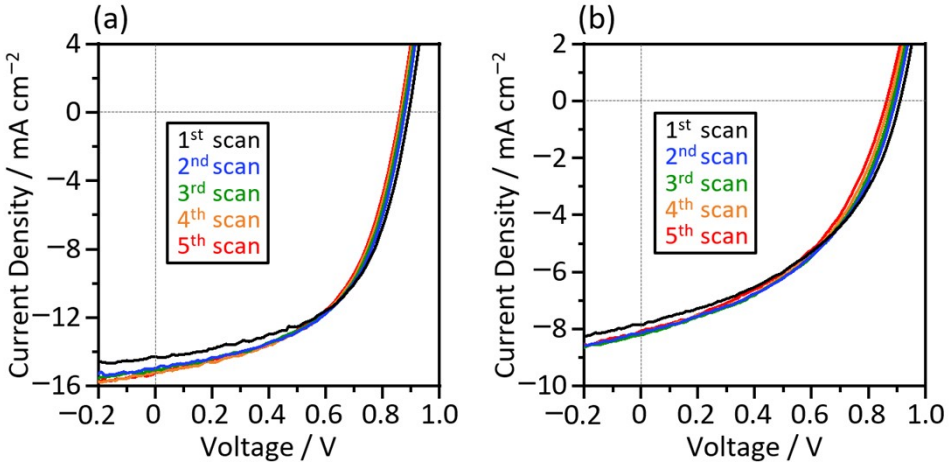

Fig. S9 *J–V* curves of PBDB-T:TT-FT-DCI based OSCs (a) and PBDB-T:TT-T-DCI based OSCs (b) after repeated scans.

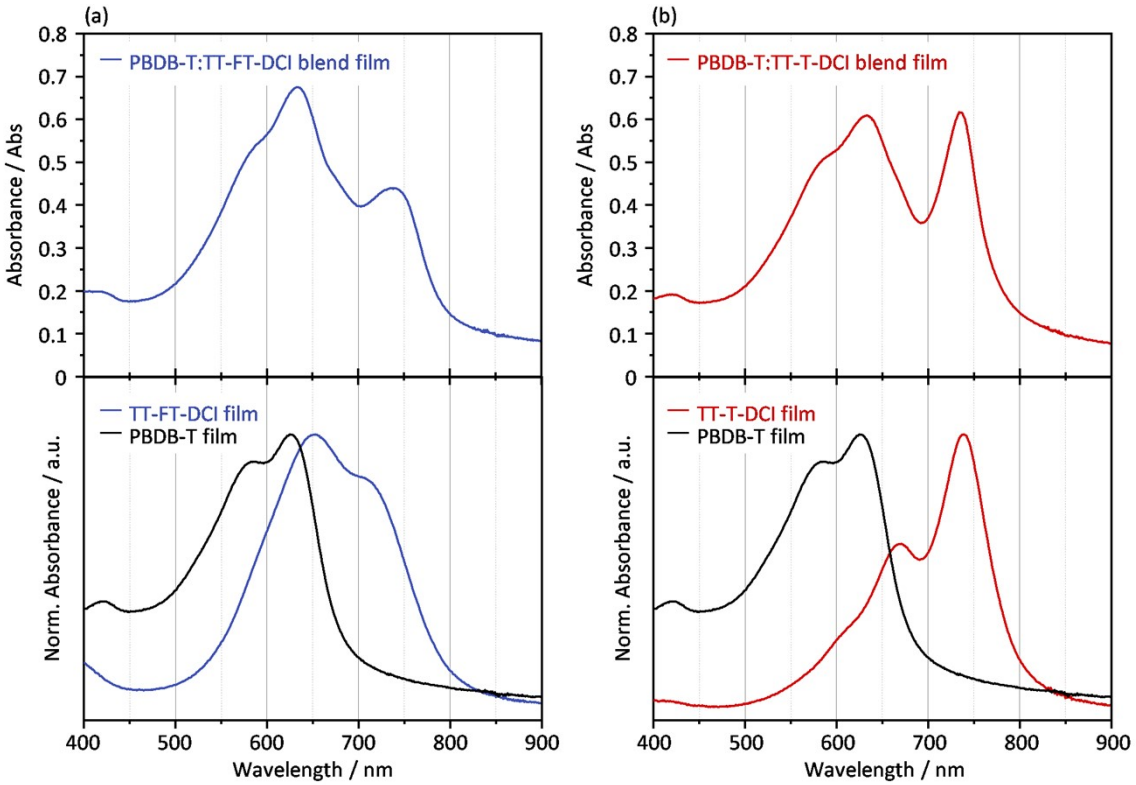

Fig. S10 UV-vis absorption spectra of blend films and neat films for (a) TT-FT-DCI and (b) TT-T-DCI.

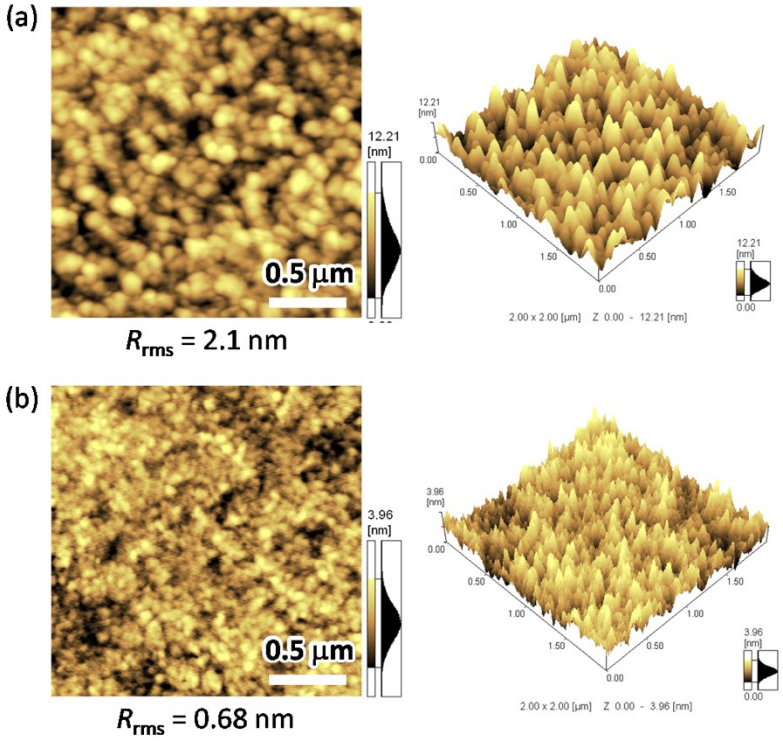

Fig. S11 AFM images of (a) PBDB-T:TT-FT-DCI and (b) PBDB-T:TT-T-DCI films.

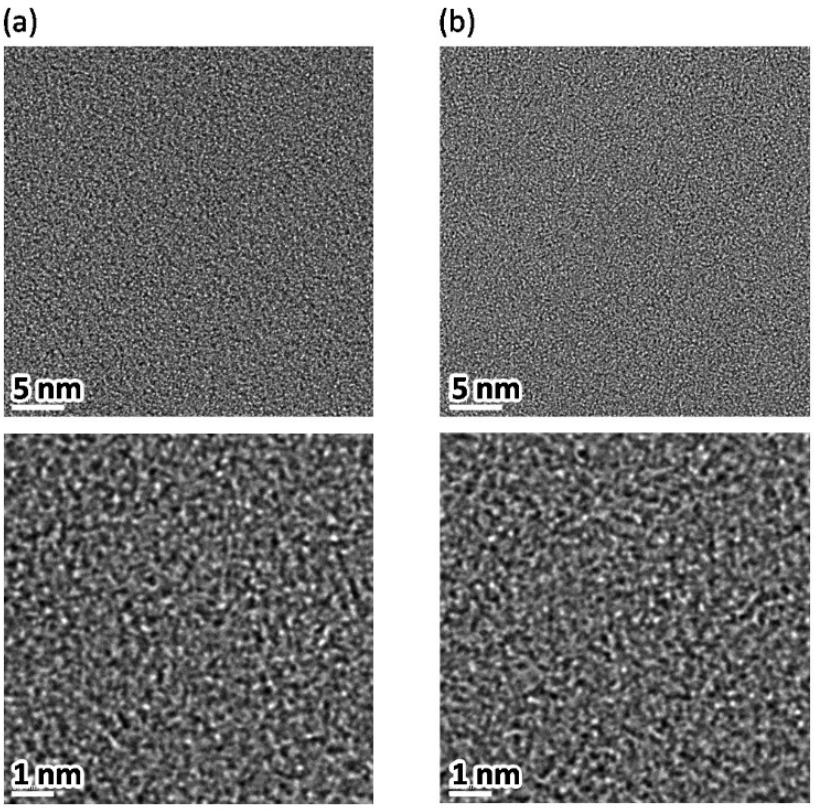

Fig. S12 Transmission electron microscopy (TEM) images of active layer for PBDB-T:TT-FT-DCI (a) and PBDB-T:TT-T-DCI (b).

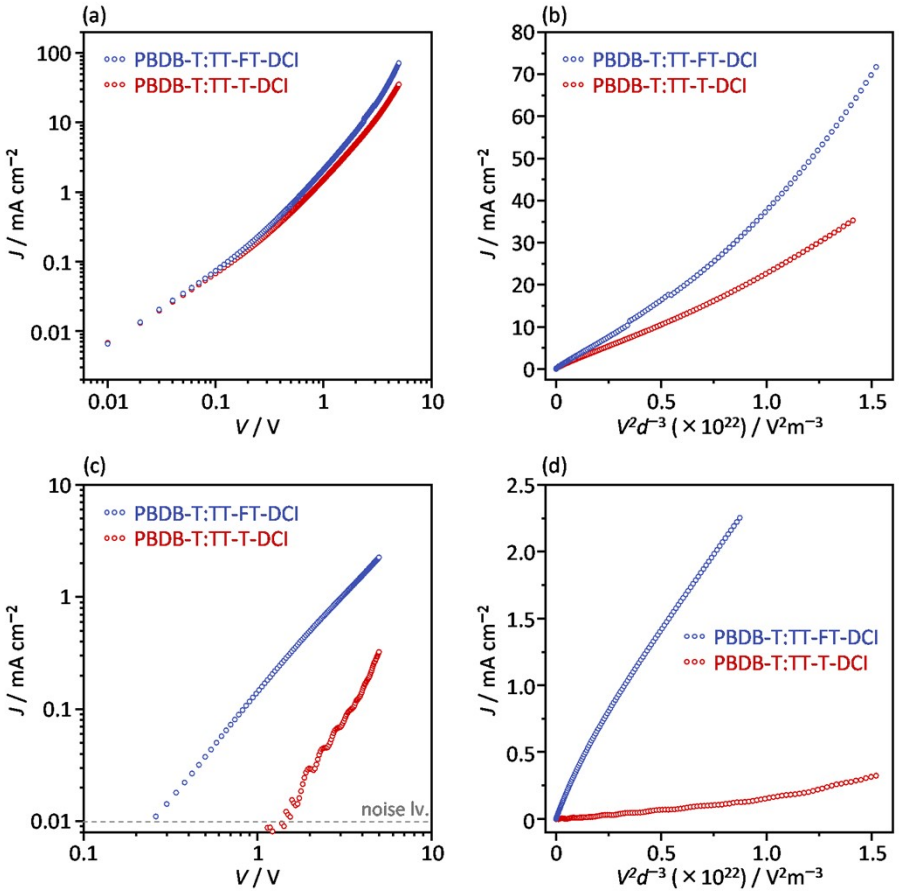

Fig. S13 *J–V* plots and $J–V^2d^{-3}$ plots for (a, b) hole only device of ITO/PEDOT:PSS/PBDB-T:acceptor/MoO_3/Ag, and (c, d) electron only device of ITO/ZnO/PBDB-T:acceptor/Ca/Al.

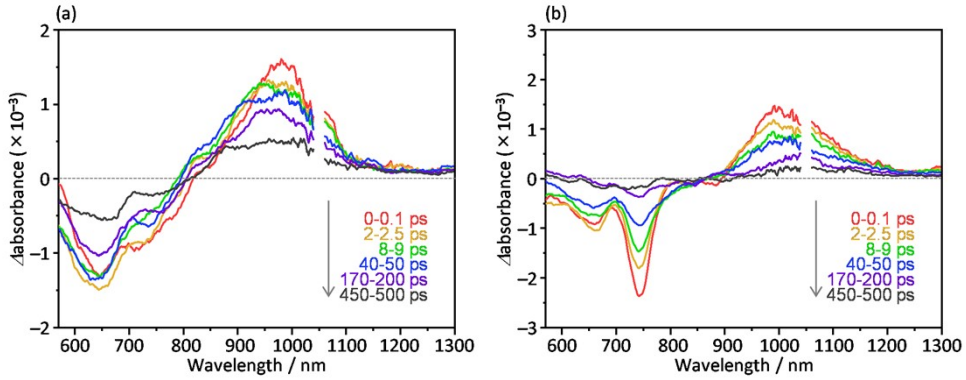

Fig. S14 Transient absorption spectra of (a) TT-FT-DCI and (b) TT-T-DCI films in the visible and NIR region.

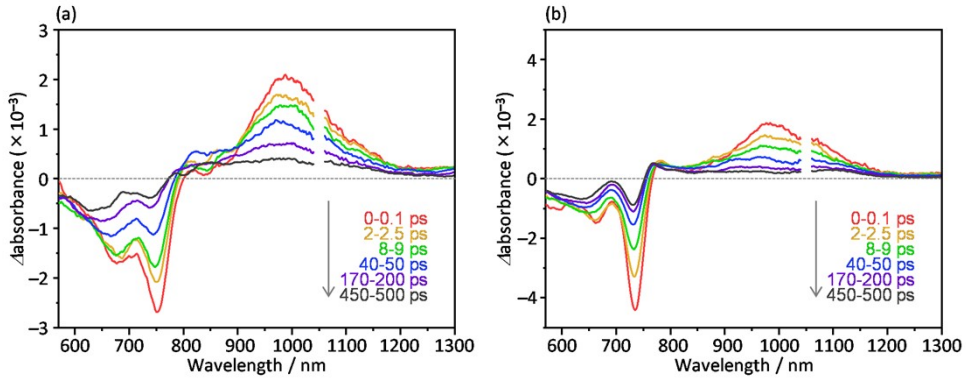

Fig. S15 Transient absorption spectra of (a) PBDB-T:TT-FT-DCI and (b) PBDB-T:TT-T-DCI films in the visible and NIR region.

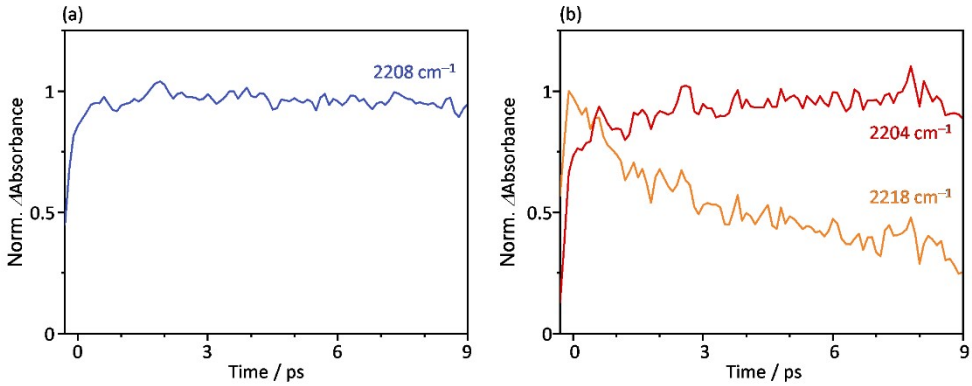

Fig. S16 Time profile of the transient absorption for (a) TT-FT-DCI at 2208 cm^{-1} and (b) TT-T-DCI at 2204 and 2218 cm^{-1} until 9 ps.

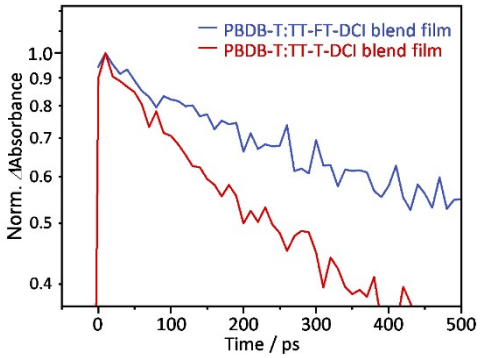

Fig. S17 Temporal profiles of transient absorption at 2191 cm^{-1} for PBDB-T:TT-FT-DCI and PBDB-T:TT-T-DCI films.

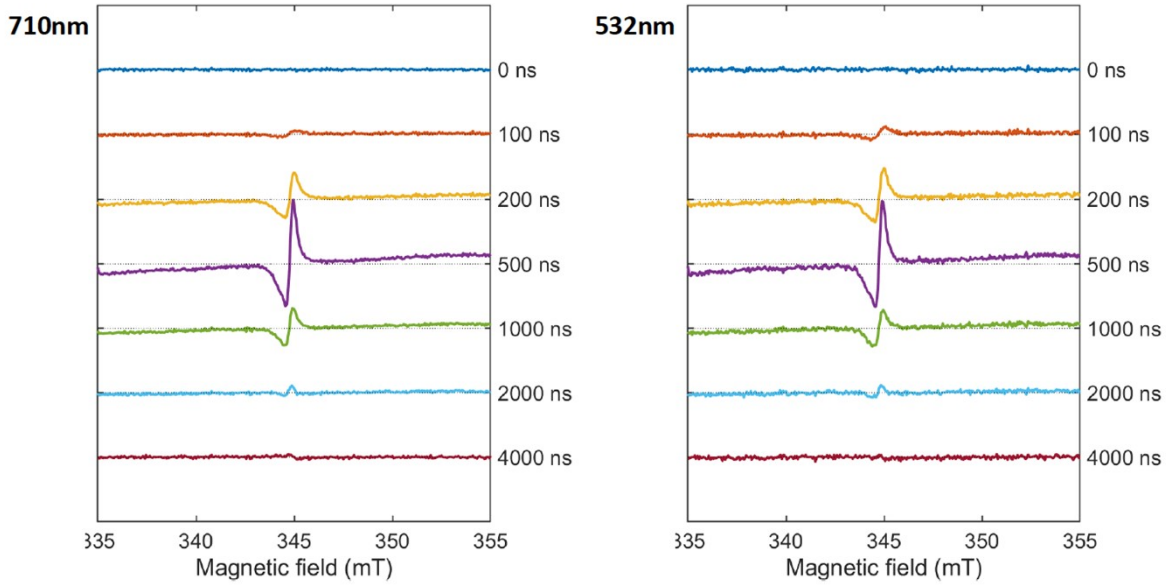

Fig. S18 Excitation wavelength (710 nm and 532 nm) effect of the TREPR spectra for different delay times observed in the numbers of cut films of the substrate/ZnO/PBDB-P:TT-FT-DCI at 80 K. This independence of the wavelength denotes that the exciton diffusions and subsequent singlet excitation energy transfer from PBDB-T to TT-FT-DCI occurred efficiently prior to the trapped CS state generations after the 532 nm laser excitations. This is because the 532 nm light is dominantly absorbed by PBDB-T, while 710 nm light is absorbed by TT-FT-DCI molecule in the blend films from the ground state absorption spectra of PBDB-T pristine film and of the PBDB-P:TT-FT-DCI blend film, as shown in Fig. S10a.

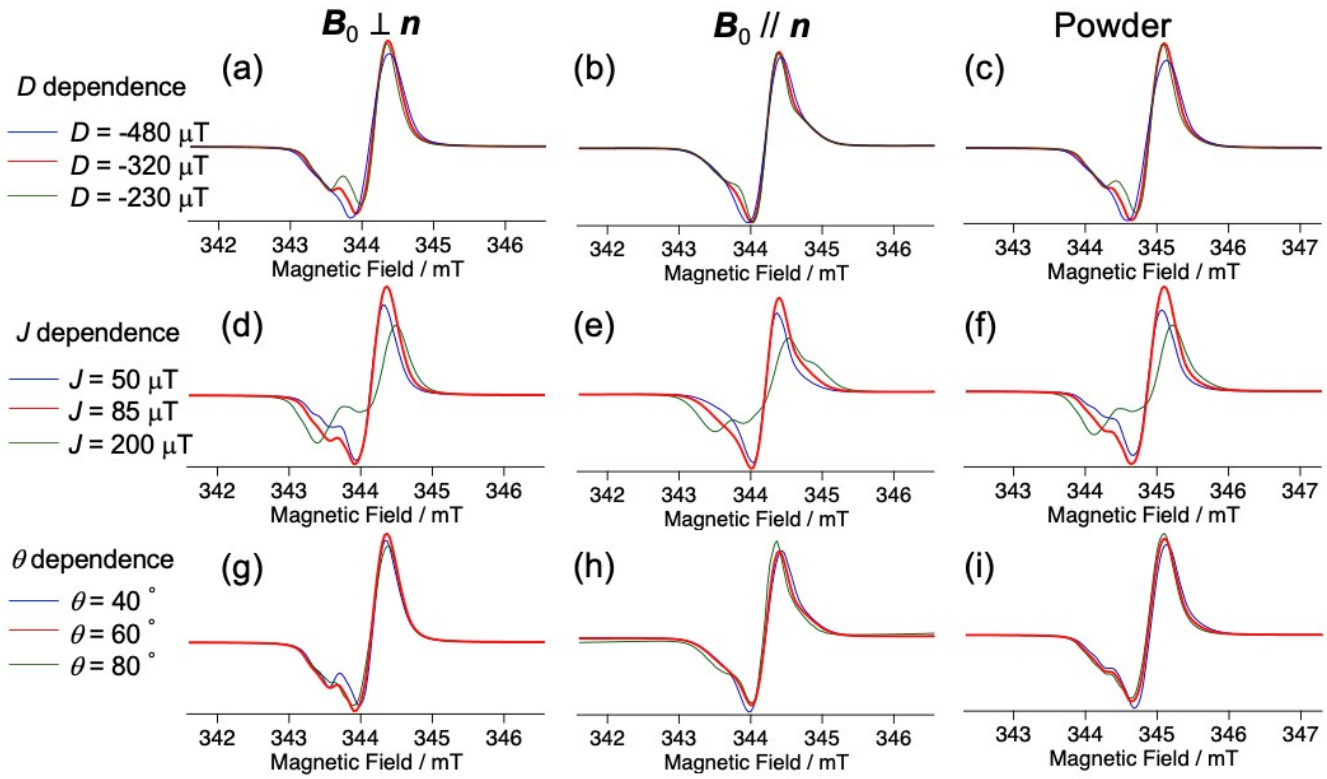

Fig. S19 Susceptivity of the input EPR parameters of the spin-polarized SCRP spectra in Fig. 10 for evaluations of the errors in Table S7 (parenthesis). The red spectra correspond to the determined parameter set in Table S7 from the red lines in Fig. 10.

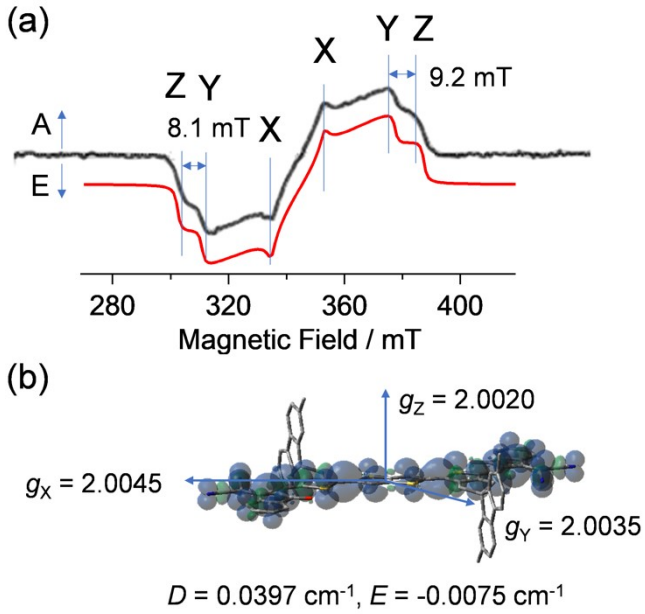

Fig. S20 (a) TREPR spectrum of the powder sample of TT-FT-DCI pristine film at 0.2 μs after the 532 nm laser irradiations at 80 K. Simulated powder pattern spin-polarized EPR spectrum of the triplet state is shown by the red line. X, Y and Z denote the resonance positions for the principal axes of the ZFS interaction. The spitting (9.2 mT) between Z and Y resonance lines is larger at the higher field than the corresponding splitting (8.1 mT) at the lower field. This is explained by the attribution of the Z principal axis to be parallel to the g_Z principal axis with g_Z = 2.0020 as the free electron in (b). This well supports the positive D value and was also consistent with the positive D^{calc} value obtained by the molecular orbital calculations in Table S6. Thus, it is concluded that the D_{ZZ} axis is perpendicular to the aromatic plane and is tilted by θ_n = 35° from the substrate normal vector (***n***) in Fig. S21d.

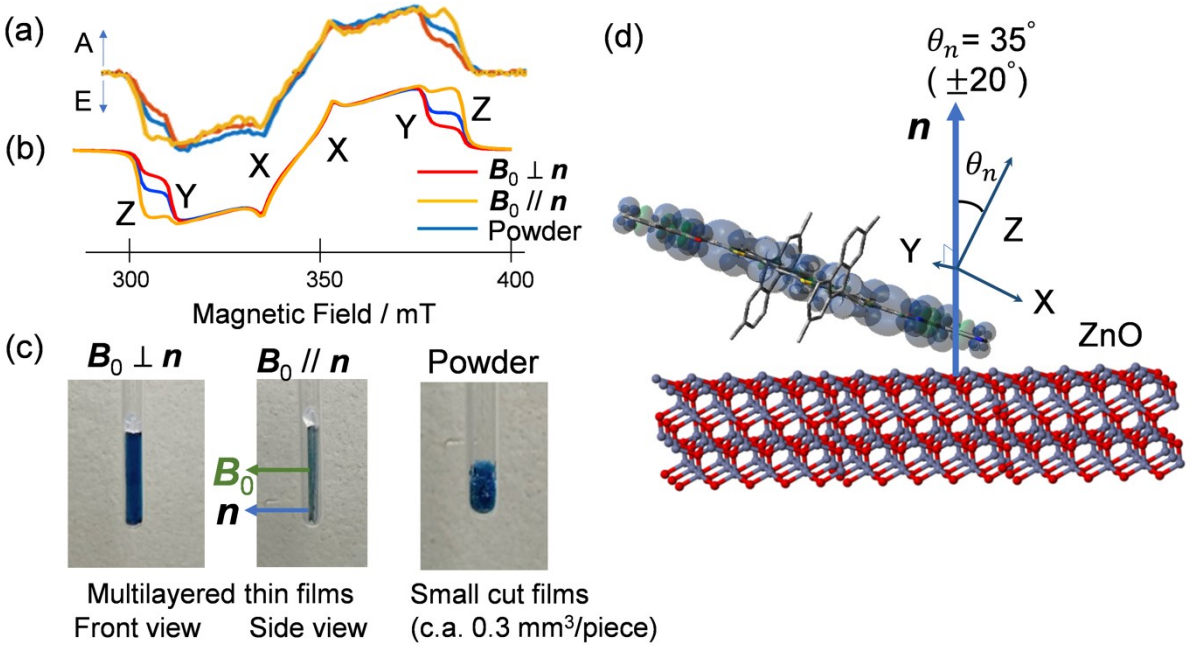

Fig. S21 TREPR spectroscopy of TT-FT-DCI pristine film. (a) Experimental TREPR spectra (0.2 μs) of the triplet excitons for the different film orientations with respect to the external magnetic field (B_0). (b) Simulations of the TREPR spectra. (c) Photos of the thin films with front view, side view and numbers of cut films, respectively. (d) Orientation of the triplet exciton with respect to the substrate normal vector (n) obtained from the simulations in (b).

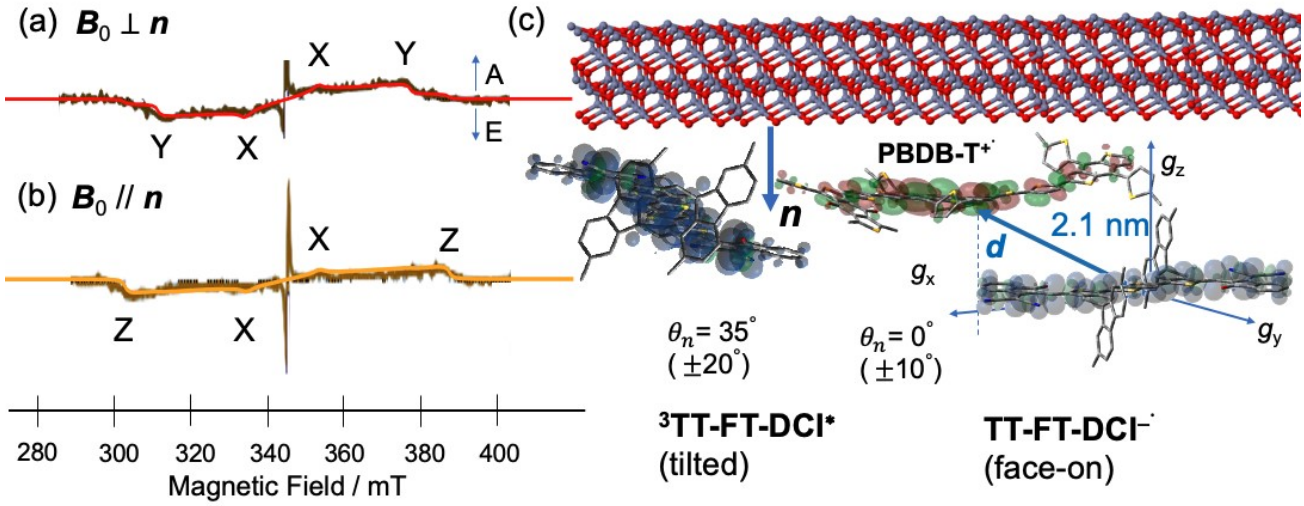

Fig. S22 (a, b) Wide range TREPR spectra of the PBDB-T:TT-FT-DCI blend film at 0.2 μs, demonstrating the 35° tilted conformation in the triplet exciton of ^{3}TT-FT-DCI*. The center E/A signals correspond to (a) and (b) in Fig. 10. (c) Difference in the molecular orientations of TT-FT-DCI between the triplet exciton and the reduced radical in the CS state. It was confirmed in the blend films that there existed the trapped triplet excitons from the entire views of the TREPR spectra in (a) and (b) which were very similar to the triplet spectra of the pristine films (Fig. S21).

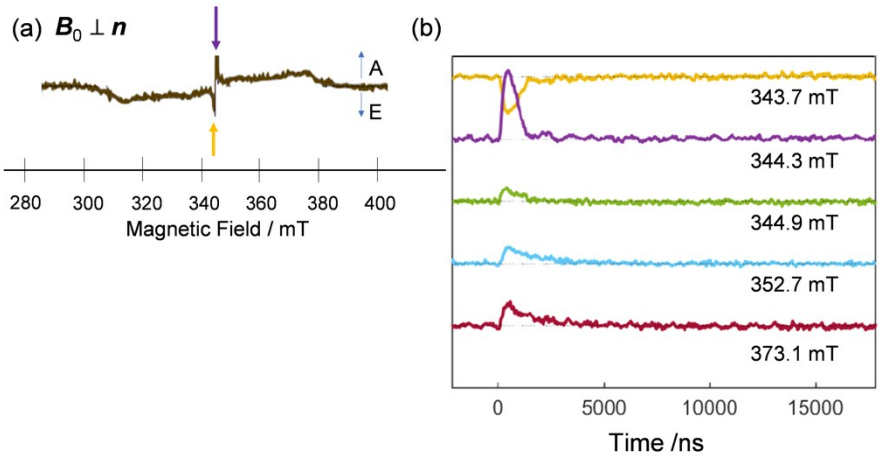

Fig. S23 (a) The TREPR spectrum of substrate/ZnO/PBDB-T:TT-FT-DCI at 80 K for B_0 perpendicular to the normal vector n. (b) The time profiles of the TREPR signals of the SCRP polarizations are shown by yellow and purple lines at lower and at higher fields indicated by the arrows in (a). Rabi oscillations around 1000 ns are identified in the SCRP signals while the quantum beats were not detected for the triplet exciton signals at the higher field positions. The microwave power was 2.5 mW.

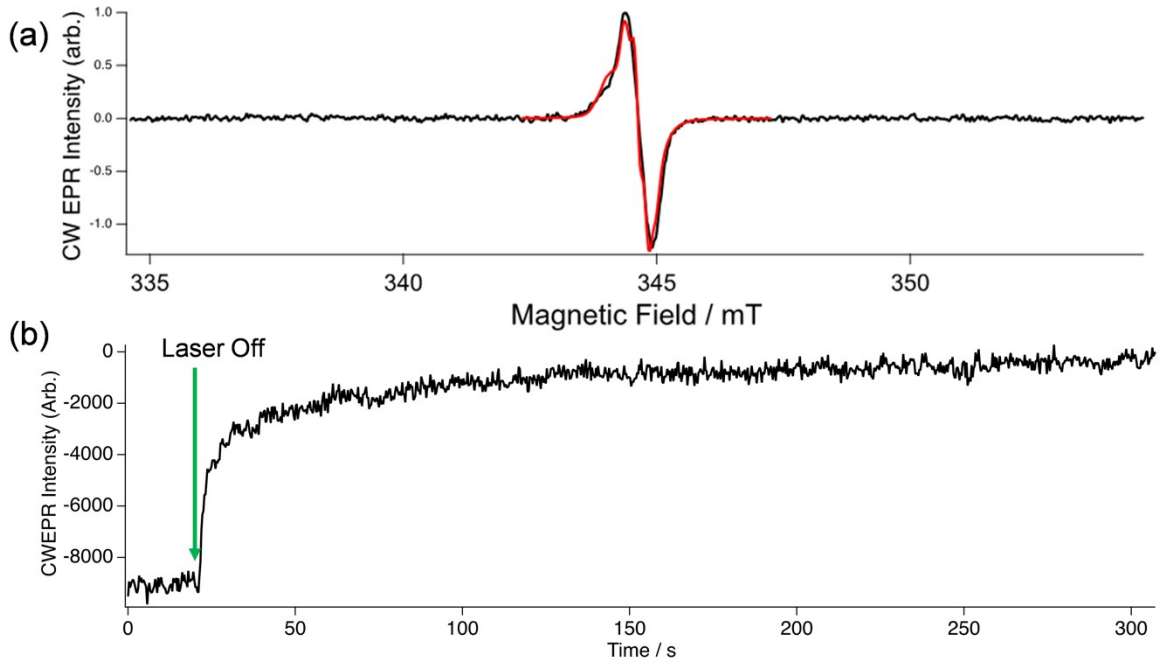

Fig. S24 Field-modulation CW-EPR spectroscopy of small cut films of the substrate/ZnO/PBDB-T:TT-FT-DCI under 10 Hz 532 nm laser irradiation with 10 mW at 80 K. (a) The field modulated EPR spectrum was observed during the laser irradiations. Microwave frequency was 9660.629 MHz. The field modulation width was 0.2 mT with the frequency of 100 kHz. The red line was computed as a separated radical pair composed of PBDB-$T^{+\cdot}$ and TT-FT-$DCI^{-\cdot}$ in Table SX2 with D = –0.2 mT (r = 2.5 nm) and with J = 0. (b) The time trace of the field modulated EPR intensity after turning the laser off at 20 seconds at 344.5 mT in (a). The time constant was 20.48 ms.

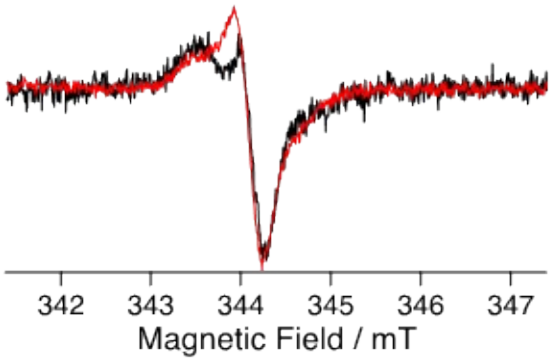

Fig. S25 Field-modulation CW-EPR spectroscopy of substrate/ZnO/PBDB-T:TT-FT-DCI under 10 Hz 532 nm laser irradiation with 10 mW at 80 K for the multilayered thin films in Fig. 10. The black spectrum was obtained for $B_0 \perp n$, while the red line was observed for B_0 // n. The enhanced EPR intensity at lower field side in the black line denotes that the contributions from g_x = 2.0047 and g_y = 2.0033 of TT-FT-$DCI^{-\cdot}$ are stronger than the contribution from g_z = 2.0020, as in (a) and (b) of Fig. 10. This is thus rationalized by the face-on conformation in the accumulated electrons, specifying that the long-lived charges are located nearby the ZnO/active layer interface, as the transient CS states reside, as shown in (b) of Fig. 11. The field modulation width was 0.2 mT with the frequency of 100 kHz.

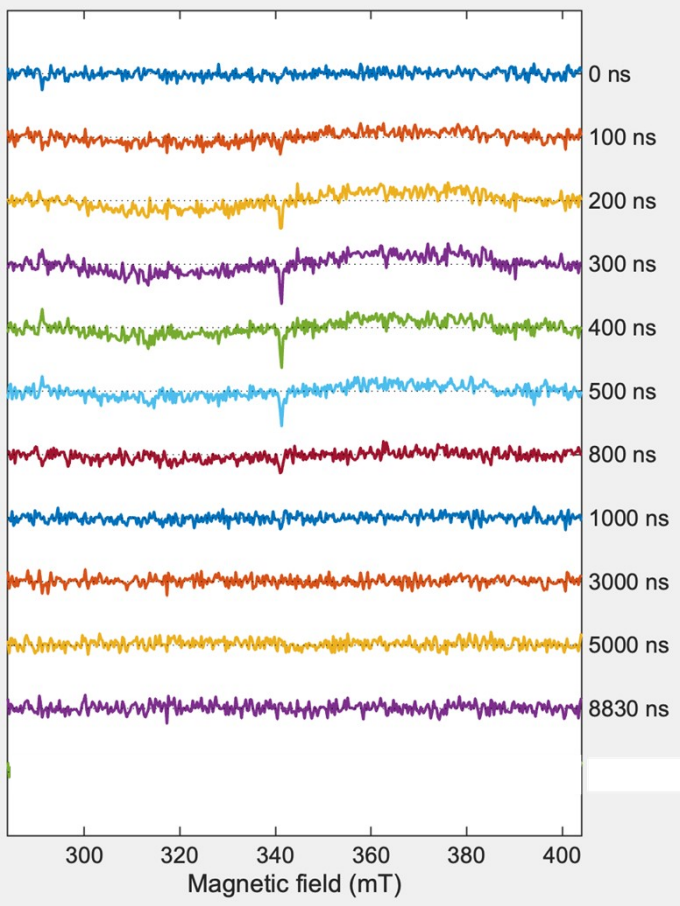

Fig. S26 TREPR spectra of substrate/ZnO/PBDB-T:TT-FT-DCI at room temperature by the 532 nm irradiations. The E/A polarized SCRP spectra in Fig. S18 are absent, indicating the de-trapping of the CS state at this elevated temperature. The emissive sharp signal at g = 2.003 is possibly originating from the triplet excitons (^{3}TT-FT-DCI*) undergoing the exciton diffusions at the elevated temperature because the weak E/A polarized trapped triplet EPR signals are also observed as in Fig. 19. One plausible scenario in the present 10 Hz repetitive laser irradiation experiments at 10 mW in Fig. 11b is that further electron de-trapping from the present CS state is blocked due to the light-induced long-lived accumulated charges nearby cathode at 80 K (Fig. S24).

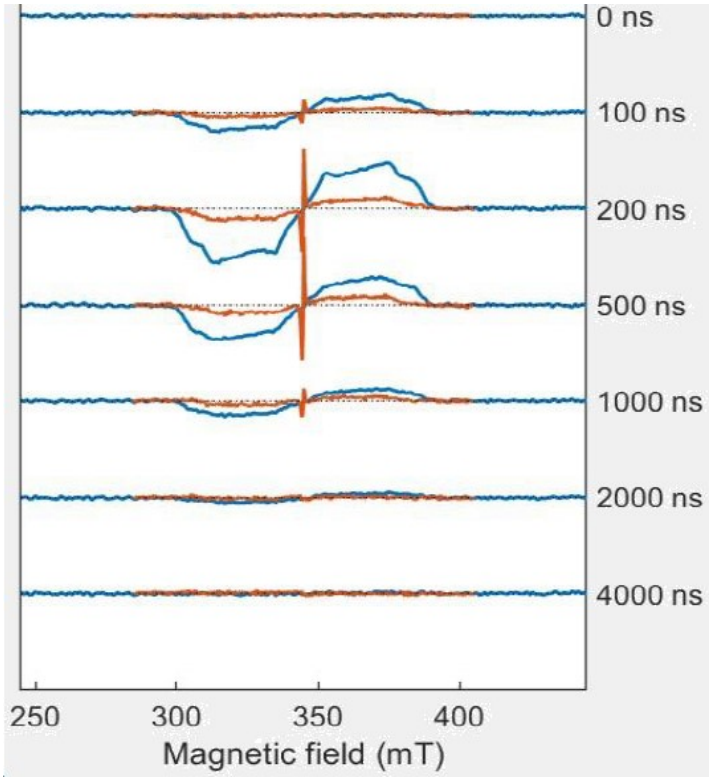

Fig. S27 Comparison between the TREPR spectra of substrate/ZnO/PBDB-T:TT-FT-DCI (red lines) and the TT-FT-DCI pristine film (blue lines) at 80 K by the 532 nm irradiations for the numbers of cut films. The experimental setup was unchanged for the two TREPR measurements. The five-times smaller triplet EPR intensity in the PBDB-P:TT-FT-DCI blend than that in the pristine sample demonstrates that the significant amount of the electrons and holes were generated instead of the triplet excitons due to the homogeneous donor/acceptor miscibility in the entire photoactive layers. The signal intensities of the triplet excitons were much weaker than those in the pristine films. These reduced intensities denote that significant amount of the electrons and holes were generated instead of the triplet excitons due to the homogeneous donor/acceptor miscibility in the entire photoactive layers of the blend films.[6] This well supports the argument that the exciton diffusions and subsequent singlet excitation energy transfer from PBDB-T to TT-FT-DCI occurred efficiently prior to the trapped CS state generations after the 532 nm laser excitations from the essential independence of the excitation wavelength on the TREPR spectrum (Fig. S18).

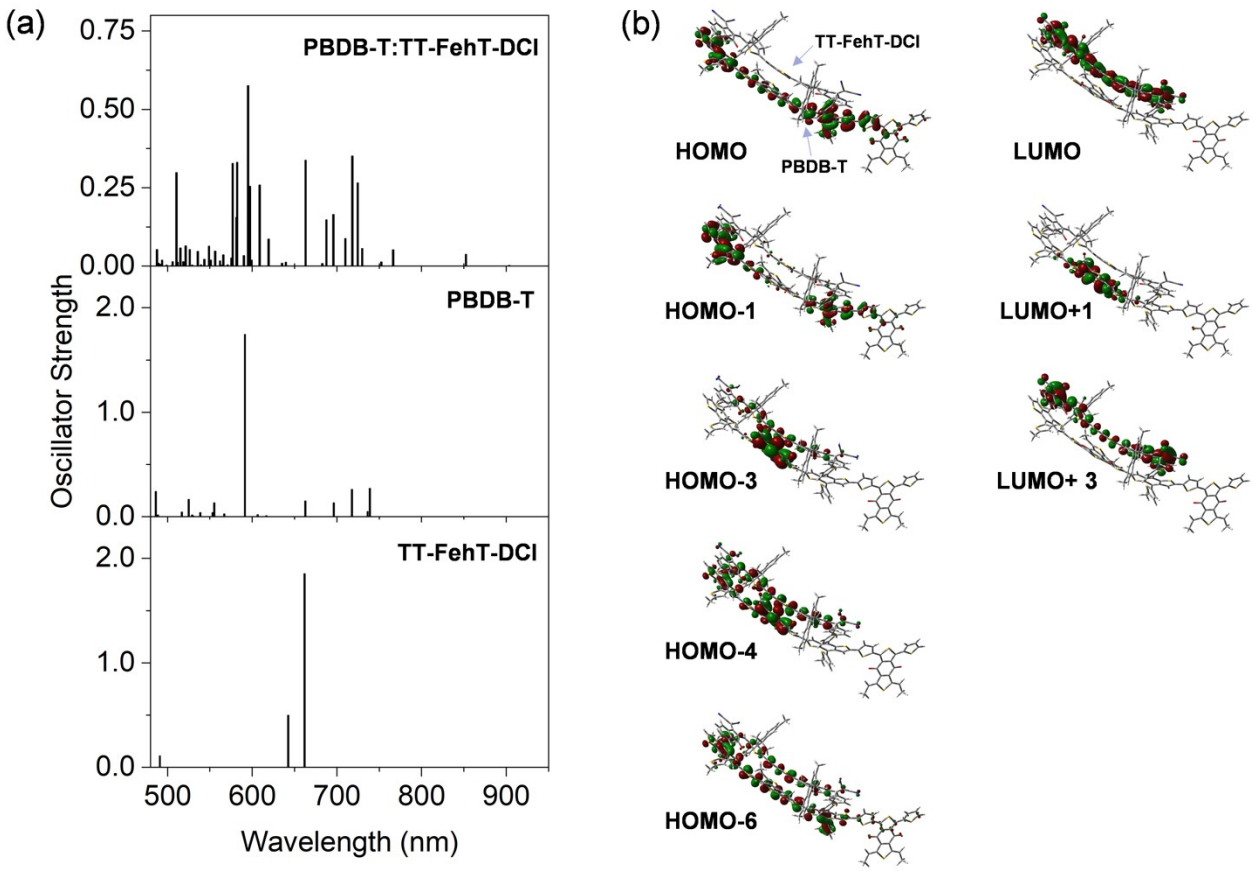

Fig. S28 (a) Electronic transitions and (b) corresponding molecular orbitals of PBDB-T:TT-FT-DCI model complex, PBDB-T model, and TT-FT(m)-DCI. The details for transitions from 1st to 6th excitations are listed in Table S8.

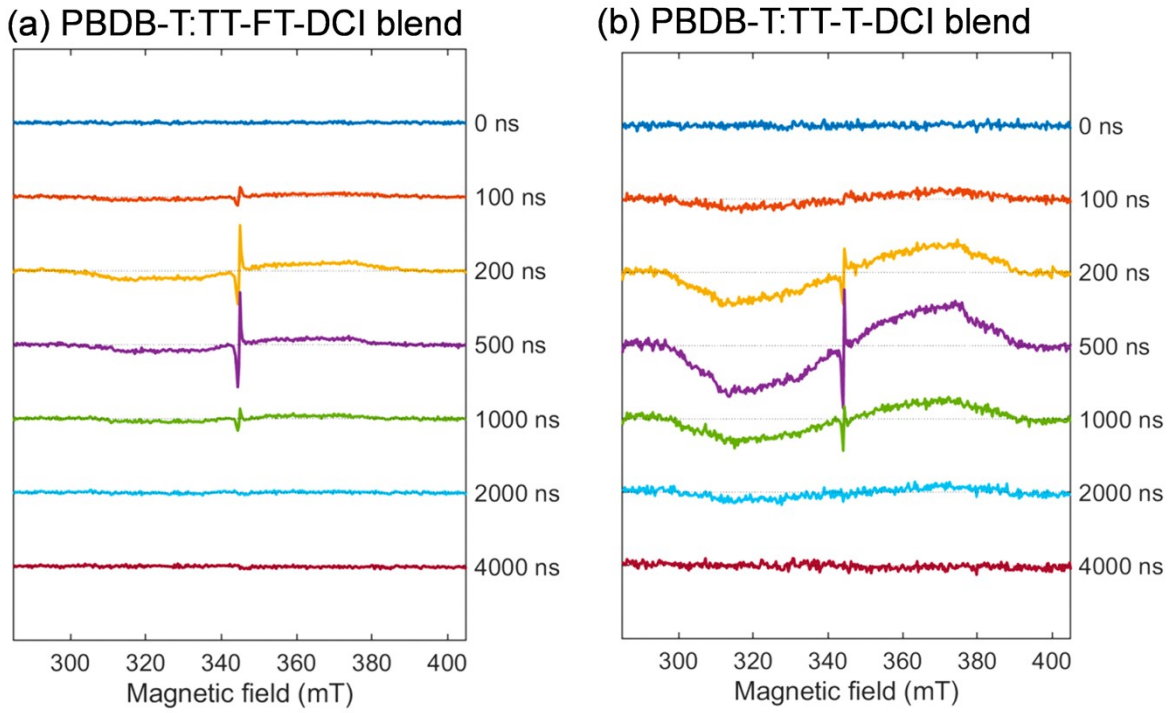

Fig. S29 Comparison between the TREPR spectra of substrate/ZnO/PBDB-T:TT-FT-DCI (a) and substrate/ZnO/PBDB-P:TT-T-DCI (b) obtained by the 532 laser irradiations of the numbers of cut films at 80 K.

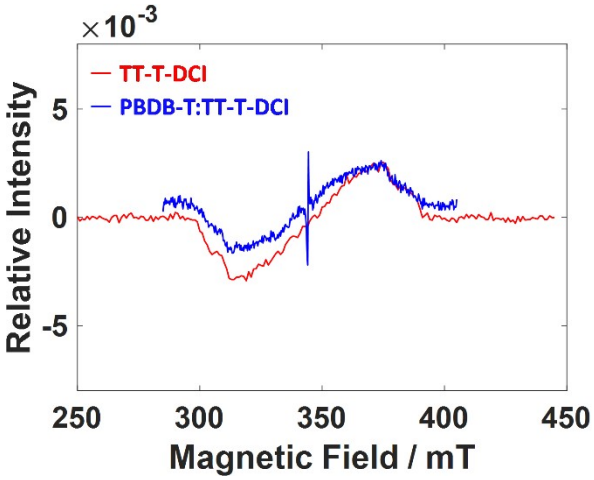

Fig. S30 Comparison of the TREPR intensities between the substrate/ZnO/PBDB-T:TT-T-DCI (blue) and the TT-T-DCI pristine film (red) at 80 K by the 532 nm irradiations for the numbers of cut films. The triplet exciton signal intensity was almost unchanged by the blend of the donor molecules, denoting the poorer donor/acceptor miscibility to generate the charges.

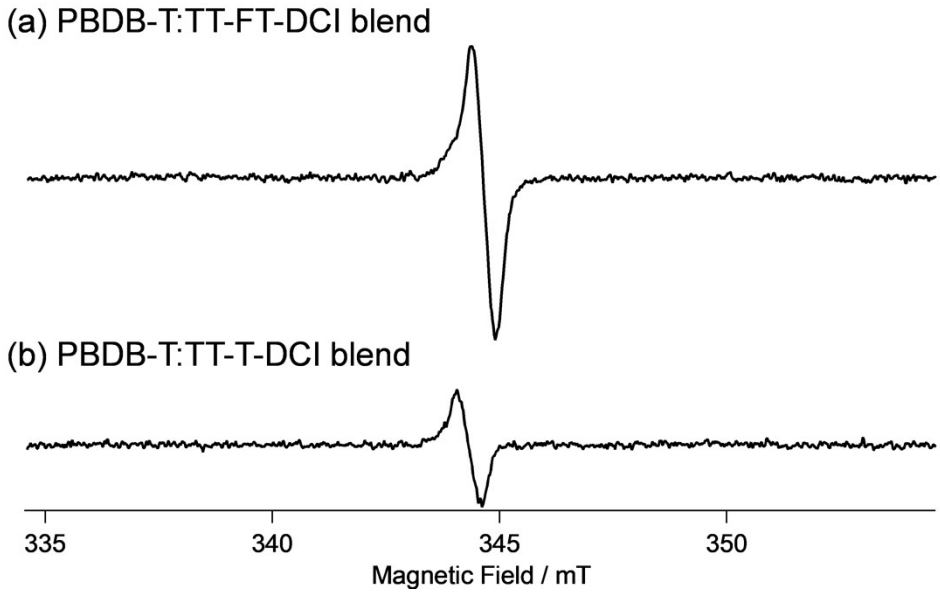

Fig. S31 Comparison between the field modulated EPR spectra of substrate/ZnO/PBDB-T:TT-FT-DCI (a) and substrate/ZnO/PBDB-T:TT-T-DCI (b) obtained by 532 laser irradiations of the numbers of cut films at 80 K. Microwave frequency was 9644.727 MHz in (a) and 9651.543 MHz in (b). The field modulation width was 0.4 mT with the frequency of 100 kHz.

Table S1 Solubilities of compounds.

compounds	solubilities / mg mL^{-1}		
	chloroform	chlorobenzene	1,2-dichlorobenzene
TT-FT-DCI	> 10	> 10	> 10
TT-T-DCI	8.6	1.6	3.0
TT-T(bo)-DCI	1.3	0.5	0.5
TT-T(eh)-DCI	0.1	(0.03)	0.1

Table S2 OSC fabrication conditions and characteristics of PBDB-T/TT-FT-DCI based devices.

D:A [a]	solvent [b]	conc. [c] / mg mL^{-1}	DIO [d] / vol%	rotation / rpm	T_a [e] / °C	PCE / %	J_{sc} / mAcm^{-2}	V_{oc} / V	FF / %
1:1	CB	20	-	1000	-	2.94	9.21	0.86	37
1:1	CB	20	-	1000	120	2.11	6.98	0.74	41
1:1	CB	20	0.5	1000	-	4.14	10.41	0.89	45
1:1	CB	20	0.5	1000	120	3.36	10.17	0.78	42
1.5:1	CB	20	0.5	1000	-	2.65	7.33	0.89	41
1:1	CB	20	0.5	1000	-	3.82	10.18	0.88	42
1:1.5	CB	20	0.5	1000	-	4.53	10.92	0.88	47
1.5:1	DCB	20	0.5	1000	-	2.85	7.99	0.85	42
1:1	DCB	20	0.5	1000	-	5.82	11.23	0.90	58
1:1.5	DCB	20	0.5	1000	-	4.93	9.49	0.89	58
1:1	DCB	20	-	1000	-	4.03	9.10	0.87	51
1:1	DCB	20	1	1000	-	5.66	10.73	0.90	59
1:1	DCB	20	2	1000	-	5.37	11.07	0.90	54
1:1	DCB	20	3	1000	-	4.93	10.84	0.90	50
1:1	DCB	20	0.5	600	-	4.75	10.66	0.89	50
1:1	DCB	20	0.5	800	-	5.18	10.67	0.90	54
1:1	DCB	20	0.5	1500	-	4.71	9.53	0.89	55
1:1	DCB	16	0.5	1000	-	5.45	10.47	0.91	57
1:1	**DCB**	**20**	**0.5**	**1000**	**-**	**6.19**	**12.15**	**0.90**	**57**
1:1	DCB	24	0.5	1000	-	5.08	10.30	0.90	55

[a] Donor:acceptor weight ratio. [b] Process solvent (CB = chlorobenzene, DCB = 1,2-dichlorobenzene). [c] Concentration of total donor:acceptor weight. [d] Volume ratio. [e] Thermal annealing temperature in N_2 for 10 min.

Table S3 OSC fabrication conditions and characteristics of PBDB-T/TT-T-DCI based devices.

D:A [a]	solvent [b]	conc. [c] / mg mL^{-1}	DIO [d] / vol%	rotation / rpm	T_a [e] / °C	PCE / %	J_{sc} / mAcm^{-2}	V_{oc} / V	FF / %
1:1	DCB	20	-	1000	-	0.22	0.88	0.77	32
1:1	DCB	20	0.5	1000	-	0.09	0.77	0.43	29
1:1	CF	10	-	1000	-	0.76	2.77	0.72	38
1:1	CF	10	-	1000	130	0.81	3.19	0.70	36
1:1	CF	10	0.5	1000	-	1.23	4.07	0.79	38
2:1	CF	10	0.5	1000	-	1.36	4.11	0.80	41
1.5:1	CF	10	0.5	1000	-	1.62	4.63	0.86	41
1:1.5	CF	10	0.5	1000	-	0.83	2.51	0.80	41
1:2	CF	10	0.5	1000	-	0.46	2.47	0.56	33
1.5:1	CF	12	0.5	1000	-	1.15	3.71	0.79	39
1.5:1	**CF**	**8**	**0.5**	**1000**	**-**	**2.46**	**6.39**	**0.92**	**42**
1.5:1	CF	6	0.5	1000	-	1.43	4.34	0.83	40
1.5:1	CF	8	0.5	1200	-	1.71	4.73	0.85	43
1.5:1	CF	8	0.5	800	-	1.84	5.00	0.89	41
1.5:1	CF	8	0.5	600	-	1.77	4.86	0.88	42

[a] Donor:acceptor weight ratio. [b] Process solvent (CB = chlorobenzene, DCB = 1,2-dichlorobenzene). [c] Concentration of total donor:acceptor weight. [d] Volume ratio. [e] Thermal annealing temperature in N_2 for 10 min.

Table S4 OSC characteristics of optimized PBDB-T:TT-FT-DCI-based devices.

Run	PCE / %	J_{SC} / mA cm^{-2}	V_{OC} / V	FF / %
1	7.13	14.30	0.89	56
2	7.11	15.16	0.89	53
3	7.06	15.02	0.88	53
4	6.99	15.03	0.89	52
5	6.79	14.58	0.89	52
average	7.02 ± 0.11	14.82 ± 0.30	0.89 ± 0.00	53 ± 1

Table S5 OSC characteristics of optimized PBDB-T:TT-T-DCI-based devices.

Run	PCE / %	J_{SC} / mA cm^{-2}	V_{OC} / V	FF / %
1	3.41	8.22	0.91	46
2	3.18	7.85	0.91	44
3	3.12	7.57	0.90	46
4	2.96	7.84	0.90	42
5	2.74	6.90	0.90	44
average	3.08 ± 0.20	7.68 ± 0.40	0.90 ± 0.00	44 ± 1

Table S6 EPR parameters of the triplet excitons of TT-FT-DCI.

Dipolar coupling constants	g-tensor (principal values)	Anisotropy in the S_1-T_1 intersystem crossing	Calculated raw matrices of D_{SS} and D_{SO} / cm^{-1}	Calculated dipolar coupling parameters / cm^{-1}
D = 0.0397 E = -0.0075	g_Z = 2.0020 g_Y = 2.0035 g_X = 2.0045	p_X = 0.52 p_Y = 0.48 p_Z = 0.00	$\mathbf{D}_{SS} = \begin{pmatrix} -0.013273 & 0.002800 & 0.001265 \\ 0.002800 & -0.000112 & 0.001117 \\ 0.001265 & 0.001117 & 0.013385 \end{pmatrix}$ $\mathbf{D}_{SO} = \begin{pmatrix} -0.005128 & -0.000594 & 0.000482 \\ -0.000594 & -0.003946 & 0.000360 \\ 0.000482 & 0.000360 & 0.000164 \end{pmatrix}$	D^{calc} = 0.0251 E^{calc} = -0.0075

Table S7 TREPR parameters of the photoinduced CS states of PBDB-T:TT-FT-DCI blends.

g-tensor (principal values in PBDB-$T^{+\cdot}$ [a])	g-tensor (principal values in TT-FT-$DCI^{-\cdot}$) [c]	Dipolar coupling constant	Dipolar angles from the g-principal axes in TT-FT-$DCI^{-\cdot}$	Exchange coupling	Orientation angles of TT-FT-$DCI^{-\cdot}$ with respect to the substrate normal vector
g_z = 2.0019 [b] g_y = 2.0025 [b] g_x = 2.0030 [b]	g_Z = 2.0020 g_Y = 2.0033 g_X = 2.0047	D = -0.32 ($\pm$ 0.10) mT	θ_d = 60 ($\pm$ 20) ° ϕ_d = 45 ($\pm$ 20) °	J = -0.85 ($\pm$ 0.10) mT	θ_n = 0° ϕ_n = arbitrary σ = 20°

a) Isotropic hyperfine couplings by two equivalent protons (a_{iso} = 0.12 mT) were also considered.

b) Taken from Ref.[7].

c) Anisotropic hyperfine couplings by two equivalent protons (a_x = 0.126 mT, a_y = 0.418 mT, a_z = 0.313 mT) were considered. Isotropic hyperfine couplings by two protons (a_{iso} = 0.2 mT) were considered. Anisotropic nitrogen hyperfine couplings by four equivalent nuclei (a_{Nx} = 0 mT, a_{Ny} = 0 mT, a_{Ny} = 0.13 mT) were considered. See below for the principal values and axes. These EPR parameters were estimated by the ORCA 5.0.2 program package for the radical anion. The other minor hyperfine couplings were treated to be included in the Lorentzian linewidth ($1/T_2 = 1.4 \times 10^7$ s^{-1}).

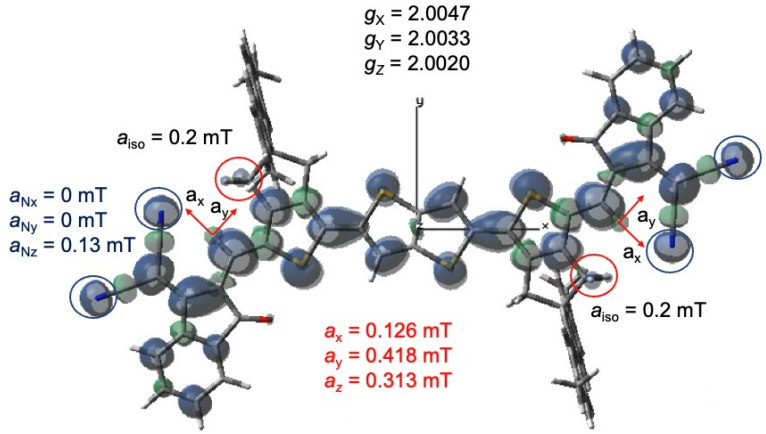

Table S8 Percentages of donor/acceptor and donor/donor transitions at the strongest absorption peak for the PBDB-T:TT-FT-DCI systems.

Transition [a]			Transition type [b]			Percentage / %
1st Exited state: f = 0.0024 at 903.45 nm						
HOMO	→	**LUMO**	**D**	→	**A**	**84**
HOMO–1	→	**LUMO**	**D**	→	**A**	**10**
HOMO–1	→	LUMO+3	D	→	A	6
2nd Exited states: f = 0.00384 at 852.33 nm						
HOMO–1	→	**LUMO**	**D**	→	**A**	**76**
HOMO	→	**LUMO+3**	**D**	→	**A**	**15**
HOMO	→	LUMO	D	→	A	9
3rd Exited states: f = 0.0521 at 766.27 nm						
HOMO	→	LUMO+1	D	→	D	100
4th Exited states: f = 0.0137 at 752.36 nm						
HOMO–1	→	LUMO+1	D	→	D	79
HOMO–4	→	**LUMO+1**	**D & A**	→	**D**	**13**
HOMO–3	→	LUMO	D & A	→	A	6
HOMO–1	→	LUMO+1	D	→	D	2
5th Exited states: f = 0.0565 at 729.80 nm						
HOMO–3	→	**LUMO+1**	**D & A**	→	**D**	**52**
HOMO–3	→	**LUMO**	**D & A**	→	**A**	**38**
HOMO–1	→	LUMO+1	D	→	D	8
HOMO–4	→	LUMO+1	D & A	→	D	3
6th Exited states: f = 0.2656 at 724.41 nm						
HOMO–4	→	**LUMO**	**D & A**	→	**A**	**81**
HOMO–3	→	LUMO	D & A	→	A	8
HOMO–1	→	LUMO+3	D	→	A	5
HOMO–6	→	LUMO	D & A	→	A	4
HOMO–3	→	LUMO+1	D & A	→	D	2

[a] The corresponding orbitals were depicted in Fig. S28. [b] "D" and "A" denote the orbitals distributed on PBDB-T model, TT-FT(m)-DCI, respectively. For "D & A" indicates the delocalized orbitals on both PBDB-T model and TT-FT(m)-DCI.

Experimental Procedures

General Information.

Column chromatography was performed on silica gel, KANTO Chemical silica gel 60N (40–50 μm). Thin-layer chromatography plates were visualized with UV light. Preparative gel-permeation chromatography (GPC) was performed on a Japan Analytical Industry LC-918 equipped with JAI-GEL 1HH/2HH. ^{1}H and ^{13}C NMR spectra were recorded on a JEOL ECS-400 spectrometer. Data are reported as follows: chemical shift in ppm (δ), multiplicity (s = singlet, d = doublet, t = triplet, m = multiplet, br = broad), coupling constant (Hz). Mass spectra were obtained on a Shimadzu GCMS-QP-5050 or Shimadzu AXIMA-TOF. High-resolution mass spectra (HRMS) were obtained at atmospheric pressure chemical ionization (APCI) using Thermo scientific LTQ Orbitrap XL. Thermogravimetric (TGA) analysis and differential scanning calorimetry (DSC) were performed under nitrogen at a heating rate of 10 °C min^{-1} with a Shimadzu TGA-50 and a Shimadzu DSC-60, respectively. UV-vis spectra were recorded on a Shimadzu UV-3600 spectrophotometer. Emission spectra were recorded using a Fluoromax-4 spectrometer in the photo-counting mode equipped with a Hamamatsu R928P photomultiplier. Cyclic voltammetry (CV) and differential pulse voltammetry (DPV) were carried out on a BAS CV-620C voltammetric analyzer using a platinum disk as the working electrode, platinum wire as the counter electrode, and Ag/$AgNO_3$ as the reference electrode at a scan rate of 100 mV s^{-1}. All spectra were obtained in spectrograde solvents. Photoelectron yield spectroscopy (PYS) was performed by Bunkoukeiki BIP-KV202GD. Low-energy inverse photoemission spectroscopy (LEIPS) was performed by Ulvac-Phi, Inc. LEIPS system. The surface structures of the deposited organic films were observed by atomic force microscopy (AFM) (Shimadzu, SPM9600). Elemental analysis was performed on a Perkin Elmer LS-50B instrument by the Elemental Analysis Section of Comprehensive Analysis Center (CAC), SANKEN, Osaka University.

OSC device fabrication and evaluation

Organic solar cells were prepared with a structure of ITO/ZnO/active layer/MoO_3/Ag.[8] ITO-coated glass substrates were first cleaned by ultrasonication in acetone, water, and 2-propanol for 10 min, respectively. ITO-coated glass substrates were then activated by ozone treatment for 1 h. ZnO layer was spin-coated using the solution of zinc acetate dihydrate (99.9%, 200 mg), ethanolamine (99%, 55 μL), and 2-methoxyethanol (99.8%, 2 mL) at 3000 rpm. and baked at 200 °C for 30 min. in air. Subsequently, the active layer was then formed by spin-coating on the ITO/ZnO electrode in a glove box. MoO_3 and Ag electrodes were evaporated on the top of active layer through a shadow mask to define the active area of the devices (0.09 cm^2) under a vacuum of 10^{-5} Pa to a thickness of 10, 80 nm determined by a quartz crystal monitor. After sealing the device from the air, the photovoltaic characteristics were measured in air under simulated AM 1.5G solar irradiation (100 mW cm^{-2}) (SAN-EI ELECTRIC, XES-301S). The current density–voltage characteristics of photovoltaic devices were measured by using a KEITHLEY 2400 source meter. The EQE spectra were measured by using a Soma Optics Ltd. S-9240. The thickness of active layer was determined by KLA Tencor Alpha-step IQ.

SCLC Measurements

Hole-only and electron-only devices were prepared with a structure of ITO/PEDOT:PSS/active layer/MoO_3/Au and ITO/ZnO/active layer/Ca/Ag, respectively.[9-11] The active layers of PBDB-T:TT-FT-DCI and PBDB-T:TT-T-DCI OSCs.were prepared using the optimized fabrication conditions. The carrier mobilities of these devices were calculated by the following equation:

$$J = \frac{9}{8}\varepsilon\varepsilon_0\mu\frac{V^2}{d^3}$$

where ε, ε_0, μ, and d are the dielectric constant of the active layer, the permittivity of free space, the carrier mobility, and the measured thickness of active layer, respectively. We used the values of $\varepsilon = 3$, $\varepsilon_0 = 8.8 \times 10^{-12}$.

X-ray diffraction measurements

X-ray diffraction (XRD) was performed using an X-ray diffractometer (Rigaku, SmartLab equipped with a a zero-dimensional scintillation counter SC-70) by Bragg-Brentano geometry with CuKα (λ = 1.5418 Å) radiation as an X-ray source with an acceleration voltage of 45 kV and a beam current of 200 mA. Out-of-plane XRD and in-plane XRD were taken by 2θ and 2$\theta\chi$ scans, respectively, between 2°–30°with scanning steps of 0.02°at a grazing incident angle (ω) of 0.2°.

Transient absorption spectroscopy

The sample films for the transient absorption (TA) measurement were prepared by drop-casting a chloroform solution of TT-FT-DCI, TT-T-DCI and their blend with PDBD-T (1:1 by wt.) onto a CaF_2 substrate. The film was set in an IR cell filled with 20 torr N_2 during the measurement. The TA measurements were carried out by the pump-probe method with a Ti:sapphire regenerative amplifier (Spectra Physics, Solstice. 90 fs duration, 1 kHz repetition rate) and optical parametric amplifiers (OPAs; Spectra Physics, TOPAS Prime). The sample was photoexcited by a 730 nm pulse (5 μJ/cm^2 pulse^{-1}, 500 Hz) from the OPA. For visible and NIR measurement, a super-continuum probe was generated by focusing a 1250 nm OPA signal into a 5 mm-thick BaF_2 plate. After the sample, the probe was dispersed with a polychromator and detected with a CMOS (UNISOKU, PK100-CX) and InGaAs (UNISOKU, NIR-PDA256) photodiode array for measurement below 1040 nm and above 1060 nm, respectively. For MIR measurement, the probe pulse was generated by the difference frequency generation between the signal and idler from the OPA in an $AgGaS_2$ crystal, and was detected with a 128-channel linear MCT array detector (Infrared Systems Development, FPAS-0144). The MIR signal was analysed after subtraction of smooth background from the spectra.

Time-resolved microwave conductivity (TRMC) measurements

TRMC was performed for the film samples placed on a quartz substrate. The microwave frequency and its power were ~9 GHz and ~3 mW, respectively. The third harmonic generation (355 nm) of a Nd:YAG laser (Continuum Inc., Surelite II, 5−8 ns pulse duration, 10 Hz) was used for the excitation (incident photon density $I_0 = 4.6 \times 10^{15}$ photons cm^{-2} pulse^{-1}). The photoconductivity ($\Delta\sigma = \Delta P_r(AP_r)^{-1}$, where A is the sensitivity factor, P_r is the reflected microwave power, and ΔP_r is the change in P_r upon exposure to light) was converted into the product of the quantum yield (φ) and sum of the charge carrier mobilities $\Sigma\mu$ (= $\mu_+ + \mu_-$) using the relationship $\varphi\Sigma\mu = \Delta\sigma(eI_0F_{light})^{-1}$, where e and F_{Light} are the electron charge and correction (or filling) factor, respectively. The experiments were performed at room temperature in the air.

Time-resolved EPR measurements

Time-resolved EPR (TREPR) spectra were measured using a Bruker EMX X-band continuous wave (CW) EPR spectrometer without magnetic field modulation at 80 K. The second harmonics of (532 nm) of a Nd:YAG laser (Continuum Minilite II, fwhm = 5 ns) were used to light excitation. Continuum optical parametric oscillators (OPO) systems (Surelite OPO Plus) pumped with a third harmonics (355 nm) of a Nd:YAG laser (Continuum, Surelite I-10, 5 ns) was used for the laser irradiations of 710 nm pulses. A laser de-polarizer (SIGMA KOKI, DEQ 1N) was placed between the laser exit and the microwave cavity. Temperature was controlled by a cryostat system (Oxford, ESR900) by using liquid nitrogen as the cryogen.

Computation of the TREPR spectra

The spin polarized EPR spectra of the excited triplet states were calculated by diagonalizing the spin Hamiltonian based on a line-shape theory for the triplet state, as reported by Levanon and coworkers[12] For the oriented multilayer samples, the substrate normal vector (***n***) was set to align with respect to the reference molecular principal axes using the polar and azimuthal angles (θ_n and ϕ_n, respectively), as reported previously.[13] Then, the angles between n and B_0 were set to be distributed by the Gaussian functions around 0 and π for $\boldsymbol{n} \parallel \boldsymbol{B}_0$ and around π/2 and –π/2 for $\boldsymbol{n} \perp \boldsymbol{B}_0$. The distribution width was defined as σ, as reported previously.[13] The SCRP polarization spectra were computed based on the singlet precursor theory reported by Hore and coworkers,[14] invoking the above-mentioned angle distribution for $\boldsymbol{n} \parallel \boldsymbol{B}_0$ and for $\boldsymbol{n} \perp \boldsymbol{B}_0$.[13] The powder pattern EPR spectra were obtained both for the triplet excitons and for the SCRPs with considering the above angle distributions within the molecular axis systems of the acceptor molecules of ^{3}TT-FT-DCI* in the exciton and of TT-FT-DCI$^{-\cdot}$ in the CS state, respectively. In Fig. 11b, the position of oxidized radical of PBDP-T$^{+\cdot}$ was set by the polar and azimuthal angles (θ_d, ϕ_d) with respect to the g-principal axis system in TT-FT-DCI$^{-\cdot}$ for the dipolar tensor orientation in the radical pair. The conformation of the g-tensor axis system of PBDP-T$^{+\cdot}$ was set to be collinear with that of g-principal axis system in TT-FT-DCI$^{-\cdot}$. The almost isotropic g-factor of PBDP-T$^{+\cdot}$ in Fig. 11d however prevents us from the identification of the conformation of the oxidized radical. The errors of the input EPR parameters (Table S7) were examined from the parameter susceptivity of the TREPR spectra in Fig. S19.

Molecular Orbital Calculations for the EPR parameters

Geometry optimizations of the ground triplet state and the reduced state of TT-FT-DCI were performed by using the density functional theory (DFT) method by B3LYP with 6-31G(d) basis sets in Gaussian 09 program package. The Cartesian coordinates of the optimized geometries are listed in the calcuation details. The alkyl substituents at the spiro-fluorene units were replaced with the methyl groups for the computations. ORCA 5.0.2 program package was employed to predict the EPR parameters (Table S6 and S7). To obtain the ZFS parameters from the ZFS tensor (D) of the triplet exciton, UKS BLYP/6-31G(d,p) keywords was employed for contributions by the spin-spin dipolar coupling tensor (D_{SS}) and by the spin-orbit coupling tensor (D_{SO}). The raw matrices of D_{SS} and D_{SO} were separately computed and $D^{calc} = D_{SS} + D_{SO}$ were diagonalized to obtain calculated dipolar coupling constants of the D^{calc} and E^{calc} values of $D^{calc} = D_{ZZ} - (D_{XX} + D_{YY})/2$ and $E^{calc} = (D_{YY} - D_{XX})/2$ from the principal values of D_{XX}, D_{YY}, and D_{ZZ} with satisfying $|E^{calc}/D^{calc}| < 1/3$.

Results for TREPR spectra of TT-FT-DCI pristine films

TREPR measurements were performed for the TT-FT-DCI pristine films by the 532 nm pulsed laser excitations at 80 K. Fig. S21(a) shows the TREPR spectra of the triplet excitons observed at different film orientations with respect to the external magnetic field (B_0) at delay times of t_d = 0.2 μs, exhibiting the electron spin polarization (ESP) by the microwave absorption (A) and emission (E). The calculated spin-polarized EPR spectra are shown in Fig. S21(b). The thin films were cut to seven pieces of ~4 mm × 20 mm films and were inserted to the EPR sample tubes with 5 mm OD (left and middle of Fig. S21(c)) as multilayered films. Thus, one can align the directions of B_0 with respect to the normal vector (n) from the substrates (as shown by the arrows at the middle of Fig. S21(c), as an example) for the red and yellow spectra in Fig. S21(a). We also prepared numbers of small cut films inserted into the EPR tube, as a powder-like sample (right in Fig. S21(c)) for the blue spectrum in Fig. S21(a).

The TREPR spectra exhibit E/E/E/A/A/A spin polarization patterns in the fine structure, which are typical to the $^3\pi\pi^*$ excited triplet states of the aromatic molecules generated by the anisotropic S_1-T_1 intersystem crossing (ISC) to the in-plane zero-field sublevels.[15,16] The outermost E/A splitting signal is stronger when B_0 is parallel to the n vector (middle of Fig. S21(c)), denoting that the Z principal axis of the zero-field splitting (ZFS) interaction is close to the n vector from the substate. This means that the out-of-plane direction causing the large splitting (Z in Fig. S21(b)) by ZFS is close to the n vector as shown in Fig. S21(d), suggesting that the π-orbital of the exciton face to the substrate. The angle between n and Z axis was determined to be $\theta_n = 35°(\pm 20°)$ and $\phi_n = 90°$ with the ZFS parameters of $D = 0.0397$ cm^{-1}, $E = -0.0075$ cm^{-1}. More details of the EPR parameters and the simulation method are described in Fig. S20 and in Table S6.[13] It was shown[6] that both of the edge-on and face-on conformers existed in the ITO/ZnO/ITIC film at the cathode interface of the NFA pristine films. In this respect, the present analysis suggests that the triplet excitons are trapped at certain tilted conformers after significant exciton diffusions and subsequent ISC processes as shown in Fig. S21(d). Free molecular rotations about the n vector were conclusive on residence of the exciton to fit the present spectra (Fig. S21(b)), although the θ_n angle was distributed with a Gaussian function width parameter of $\sigma = 40°$. Thus, the disordered morphology concluded by the XRD does not conflict with the present preferential orientations.

Preparation of Materials.
Commercially available reagents were used without purification. All reactions were carried out under a nitrogen atmosphere. **1**[17] was prepared by our previously reported procedure. Compounds **4**[18] and **6**[19] were prepared by the reference procedures.

Synthesis of 2: **1** (1.00 g, 1.52 mmol) was placed in a 300 mL two-necked round-bottomed flask and dissolved with THF (5 mL). *n*-BuLi (1.6 M hexane solution, 0.86 mL, 1.37 mmol) was added to the mixture at –78 °C. After stirring for 30 min. at –78 °C, *N*,*N*-dimethylformamide (167 mg, 2.28 mmol) was added. The mixture was gradually warmed up to room temperature. After further stirring for 1 h, the reaction was quenched by the addition of water, and the organic layer was separated. The aqueous layer was extracted with hexane, and the combined organic layer was washed with water and dried over Na_2SO_4. After removal of the solvent under reduced pressure, the residue was purified by column chromatography on silica gel (hexane/$CHCl_3$ =5/1, R_f = 0.2) to give **2** (639 mg, 69%).
Colorless solid. ^{1}H NMR (400 MHz, $CDCl_3$) δ: 9.73 (s, 1H), 7.58 (d, J = 8.0 Hz, 2H), 7.14 (d, J = 7.6 Hz, 2H), 6.97 (s, 2H), 3.45 (s, 2H), 3.08 (s, 2H), 2.54 (d, J = 6.8 Hz, 4H), 1.46-1.55 (m, 2H), 1.17-1.32 (m, 16H), 0.85 (t, J = 7.4 Hz, 12H). ^{13}C NMR (100 MHz, $CDCl_3$, TMS) δ: 180.61, 156.12, 150.40, 149.61, 141.30, 136.95, 134.10, 128.84, 122.78, 119.24, 115.71, 112.11, 61.78, 41.03, 40.03, 32.13, 28.69, 25.35, 25.28, 22.92, 14.08, 10.73. HRMS (APCI) *m/z* calcd. for $C_{36}H_{45}BrOS$ (M^+): 604; found: 604. Anal. calcd for $C_{36}H_{45}BrOS$: C 71.39, H 7.49; found: C 71.17, H 7.45.

Synthesis of 3: $Pd(PPh_3)_4$ (35 mg, 0.03 mmol) was added to a degassed test tube with screw cap containing the solution of **2** (200 mg, 0.33 mmol) and 2,5-bis(trimethylstannyl)-thieno[3,2-*b*]thiophene (70 mg, 0.15 mmol) in toluene. The resulting mixture was stirred at 110 ºC for 12 h. After removal of the solvent under reduced pressure, the residue was purified by column chromatography on silica gel (hexane/$CHCl_3$ =4/1, R_f = 0.2) to give **3** (135 mg, 76%). Orange solid. ^{1}H NMR (400 MHz, TMS) δ: 9.83 (s, 2H), 7.59 (d, J = 7.8 Hz, 4H), 7.44 (s, 2H), 7.13 (d, J = 7.8 Hz, 4H), 7.02 (s, 4H), 3.44 (s, 4H), 3.34 (s, 4H), 2.52 (d, J = 7.2 Hz, 8H), 1.45-1.54 (m, 4H), 1.13-1.28 (m, 32H), 0.81 (t, J = 6.8 Hz, 24H). ^{13}C NMR (100 MHz, TMS) δ: 181.29, 157.81, 150.85, 144.74, 141.52, 141.48, 140.70, 138.87, 137.01, 136.96, 130.70, 128.88, 122.95, 122.93, 119.26, 118.02, 62.29, 41.13, 41.06, 40.13, 32.17, 28.72, 25.37, 22.95, 14.08, 10.76. MS *m/z* calcd. for $C_{78}H_{92}O_2S_4$ (M^+): 1189; found: 1189. Anal. calcd for $C_{78}H_{92}O_2S_4$: C 78.74, H 7.79; found: C 78.52, H 7.75.

Synthesis of 5: 2,5-dibromo-3-(2-butyloctyl)thiophene (500 mg, 1.22 mmol) was placed in a 300 mL two-necked round-bottomed flask and dissolved with THF (5 mL). *n*-BuLi (1.6 M hexane solution, 0.58 mL, 0.91 mmol) was added to the mixture at –78 °C. After stirring for 30 min. at –78 °C, *N*,*N*-dimethylformamide (134 mg, 1.83 mmol) was added. The mixture was gradually warmed up to room temperature. After further stirring for 1 h, the reaction was quenched by the addition of water, and the organic layer was separated. The aqueous layer was extracted with hexane, and the combined organic layer was washed with water and dried over Na_2SO_4. After removal of the solvent under reduced pressure, the residue was purified by column chromatography on silica gel (hexane/$CHCl_3$ =4/1, R_f = 0.3) to give **5** (210 mg, 64%). Colorless liquid. ^{1}H NMR (400 MHz, $CDCl_3$) δ: 9.77 (s, 1H), 7.42 (s, 1H), 2.53 (d, J = 7.2 Hz, 2H), 1.63-1.71 (m, 1H), 1.18-1.35 (m, 16H), 0.86 (m, 6H) ^{13}C NMR (100 MHz, $CDCl_3$, TMS) δ: 181.84, 143.12, 142.65, 137.29, 122.55, 38.39, 34.04, 33.17, 32.87, 31.79, 29.56, 29.55, 28.65, 26.40, 22.93, 22.60, 14.05. HRMS (APCI) *m/z* calcd. for $C_{17}H_{28}BrOS$ ($M+H^+$): 359.1044; found: 359.1044. Anal. calcd for $C_{17}H_{27}BrOS$: C 56.82, H 7.57; found: C 56.60, H 7.51.

Synthesis of 7: Compound **7** was synthesized from **4** (60 mg, 0.13 mmol) by following the procedure used for the preparation of **3**. Yield: 66 mg (56%). Orange solid. ^{1}H NMR (400 MHz, TMS) δ: 9.87 (s, 2H), 7.59 (s, 2H), 7.42 (s, 2H), 2.78 (d, J = 7.6 Hz, 4H), 1.68-1.77 (m, 2H), 1.17-1.32 (m, 64H), 0.87 (t, J = 6.6 Hz, 12H). ^{13}C NMR (100 MHz, $CDCl_3$, TMS) δ: 182.65, 141.19, 141.07, 140.57, 140.49, 139.41, 137.53, 119.60, 38.84, 33.91, 33.35, 31.92, 31.90, 29.98, 29.67, 19.65, 29.60, 29.37, 29.32, 26.45, 22.69, 14.14.

HRMS (APCI) *m/z* calcd. for $C_{56}H_{89}O_2S_4$ ($M+H^+$): 921.5745; found: 921.5729. Anal. calcd for $C_{56}H_{88}O_2S_4$: C 72.99, H 9.63; found: C 72.87, H 9.56.

*Synthesis of **8***: Compound **8** was synthesized from **5** (65 mg, 0.14 mmol) by following the procedure used for the preparation of **3**. Yield: 72 mg (74%). Orange solid. ^{1}H NMR (400 MHz, TMS) δ: 9.87 (s, 2H), 7.59 (s, 2H), 7.43 (s, 2H), 2.79 (d, J = 6.8 Hz, 4H), 1.69-1.76 (m, 2H), 1.17-1.32 (m, 32H), 0.86 (t, J = 6.6 Hz, 12H). ^{13}C NMR (100 MHz, TMS) δ: 182.61, 141.11, 141.04, 140.53, 140.43, 139.36, 139.34, 137.44, 119.56, 38.75, 33.83, 33.27, 33.02, 31.80, 29.59, 28.61, 26.34, 22.98, 22.61, 14.08, 14.06. HRMS (APCI) *m/z* calcd. for $C_{40}H_{57}O_2S_4$ ($M+H^+$): 697.3241; found: 697.3240. Anal. calcd for $C_{40}H_{56}O_2S_4$: C 68.92, H 8.10; found: C 68.72, H 7.98.

*Synthesis of **9***: Compound **9** was synthesized from **6** (63 mg, 0.14 mmol) by following the procedure used for the preparation of **3**. Yield: 60 mg (76%). Orange solid. ^{1}H NMR (400 MHz, TMS) δ: 9.87 (s, 2H), 7.60 (s, 2H), 7.43 (s, 2H), 2.79 (d, J = 7.2 Hz, 4H), 1.65-1.73 (m, 2H), 1.20-1.39 (m, 16H), 0.87 (t, J = 6.2 Hz, 12H). ^{13}C NMR (100 MHz, TMS) δ: 182.66, 141.19, 141.06, 140.51, 140.47, 139.38, 139.35, 137.49, 119.63, 40.14, 33.51, 32.45, 28.64, 25.67, 23.01, 14.08, 10.71. HRMS (APCI) *m/z* calcd. for $C_{32}H_{41}O_2S_4$ ($M+H^+$): 585.1989; found: 585.1971. Anal. calcd for $C_{32}H_{40}O_2S_4$: C 65.71, H 6.89; found: C 65.62, H 6.91.

*Synthesis of **TT-FT-DCI***: Pyridine (100 μL) was added to solution of **3** (65 mg, 0.055 mmol) and 3-(dicyanomethylidene)indan-1-one (85 mg, 0.44 mmol) in $CHCl_3$ (5 mL) and the resulting mixture was stirred at 65 ºC for 12 h. The reaction mixture was added methanol (20 mL) and resulting precipitate was collected by filtration. The crude product was purified by column chromatography on silica gel ($CHCl_3$, R_f = 0.4), followed by further purification with reprecipitation using $CHCl_3$ and acetone to give TT-FT-DCI (63 mg, 75%). Deep blue solid. ^{1}H NMR (400 MHz, TMS) δ: 8.77 (s, 2H), 8.66 (d, J = 6.4 Hz, 2H), 7.95 (d, J = 6.0 Hz, 2H), 7.81 (m, 4H), 7.67 (s, 2H), 7.63 (d, J = 7.6 Hz, 4H), 7.21 (d, J = 7.6 Hz, 4H), 7.17 (s, 4H), 3.51 (s, 4H), 3.50 (s, 4H), 2.62 (t, J = 7.6 Hz, 8H), 1.50-1.60 (m, 8H), 1.13-1.30 (m, 40H), 0.80 (t, J = 6.2 Hz, 12H). ^{13}C NMR (100 MHz, TMS) δ: 188.51, 166.83, 151.17, 144.48, 142.63, 142.50, 141.61, 140.18, 139.87, 137.11, 136.80, 135.38, 135.12, 134.62, 134.36, 128.93, 127.57, 125.32, 123.76, 123.06, 121.48, 119.34, 119.09, 118.06, 114.55, 114.47, 61.81, 41.05, 40.76, 40.22, 32.16, 29.72, 28.73, 25.35, 23.02, 14.13, 10.77. MS *m/z* calcd. for $C_{102}H_{100}N_4O_2S_4$ (M^+): 1541; found: 1541. Anal. calcd for $C_{102}H_{100}N_4O_2S_4$: C 79.44, H 6.54, N 3.63; found: C 79.22, H 6.66, N 3.38.

*Synthesis of **TT-T-DCI***: Compound **TT-T-DCI** was synthesized from **7** (66 mg, 0.072 mmol) by following the procedure used for the preparation of **TT-FT-DCI**. Yield: 51 mg (56%). Deep blue solid. ^{1}H NMR (400 MHz, TMS) δ: 8.82 (s, 2H), 8.71 (d, J = 6.8 Hz, 2H), 7.96 (d, J = 6.8 Hz, 2H), 7.79 (m, 4H), 7.66 (s, 2H), 7.65 (s, 2H), 2.84 (d, J = 7.2 Hz, 4H), 1.75-1.82 (m, 2H), 1.19-1.33 (m, 64H), 0.85 (t, J = 7.0 Hz, 12H). HRMS (APCI) *m/z* calcd. for $C_{80}H_{97}N_4O_2S_4$ ($M+H^+$): 1273.6494; found: 1273.6492. Anal. calcd for $C_{80}H_{96}N_4O_2S_4$: C 75.43, H 7.60, N 4.40; found: C 75.32, H 7.62, N 4.61.

*Synthesis of **TT-T(bo)-DCI***: Compound **TT-T(bo)-DCI** was synthesized from **8** (50 mg, 0.072 mmol) by following the procedure used for the preparation of **TT-FT-DCI**. Yield: 51 mg (68%). Deep blue solid. ^{1}H NMR (400 MHz, TMS) δ: 8.83 (s, 2H), 8.72 (d, J = 6.6 Hz, 2H), 7.96 (d, J = 6.6 Hz, 2H), 7.79 (m, 4H), 7.66 (s, 2H), 7.65 (s, 2H), 2.85 (d, J = 7.6 Hz, 4H), 1.72-1.81 (m, 2H), 1.18-1.32 (m, 32H), 0.86 (t, J = 7.6 Hz, 12H). HRMS (APCI) *m/z* calcd. for $C_{64}H_{65}N_4O_2S_4$ ($M+H^+$): 1049.3990; found: 1040.3992.

*Synthesis of **TT-T(eh)-DCI***: Compound **TT-T(eh)-DCI** was synthesized from **9** (20 mg, 0.034 mmol) by following the procedure used for the preparation of **TT-FT-DCI**. Yield: 15 mg (47%). Deep blue solid. ^{1}H NMR (400 MHz, TMS) δ: 8.83 (s, 2H), 8.72 (d, J = 6.6 Hz, 2H), 7.96 (d, J = 6.6 Hz, 2H), 7.79 (m, 4H), 7.67 (s, 2H), 7.66 (s, 2H), 2.84 (d, J = 7.6 Hz, 4H), 1.72-1.81 (br, 2H), 1.18-1.32 (m, 16H), 0.88 (m, 12H). HRMS (APCI) *m/z* calcd. for $C_{56}H_{49}N_4O_2S_4$ ($M+H^+$): 937.2738; found: 937.2712.

NMR Spectra

^{1}H NMR spectrum of **2**

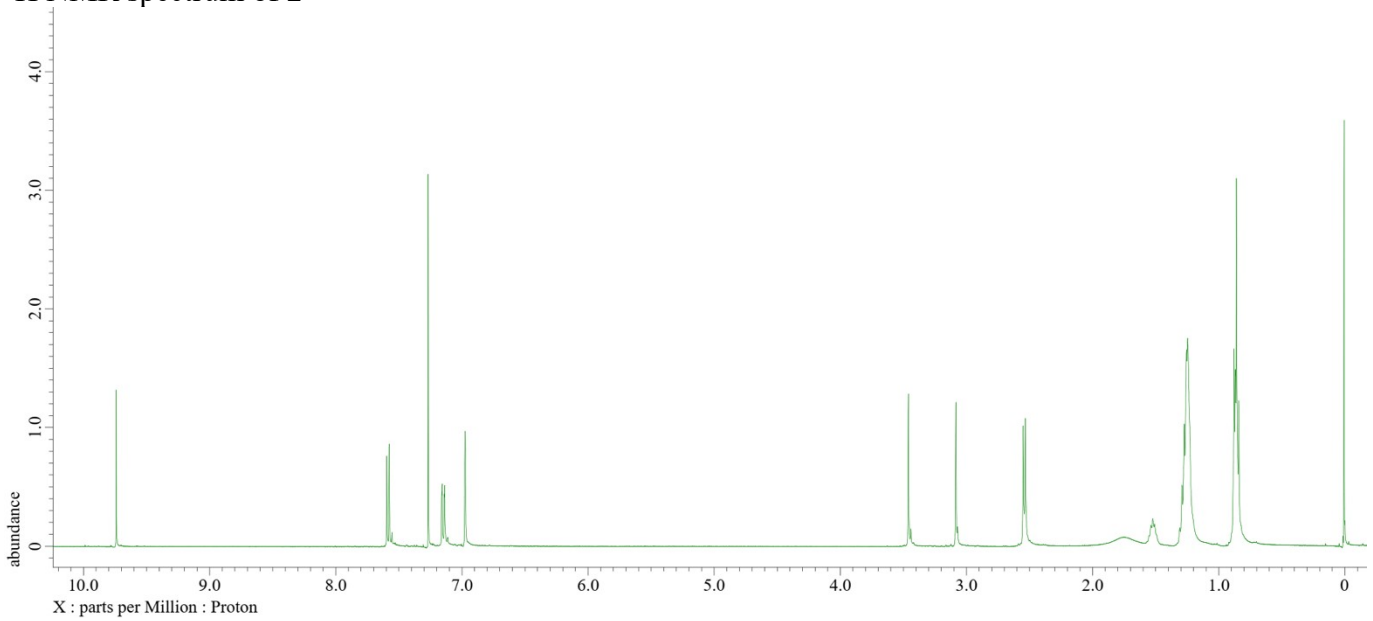

^{13}C NMR spectrum of **2**

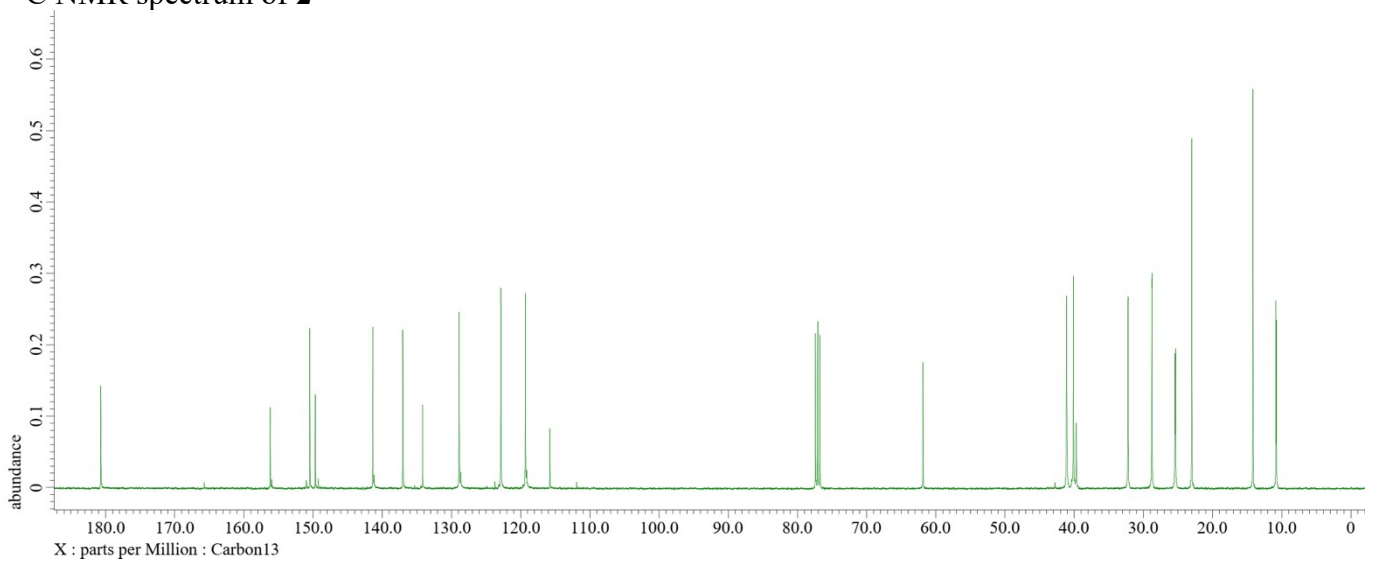

^{1}H NMR spectrum of **3**

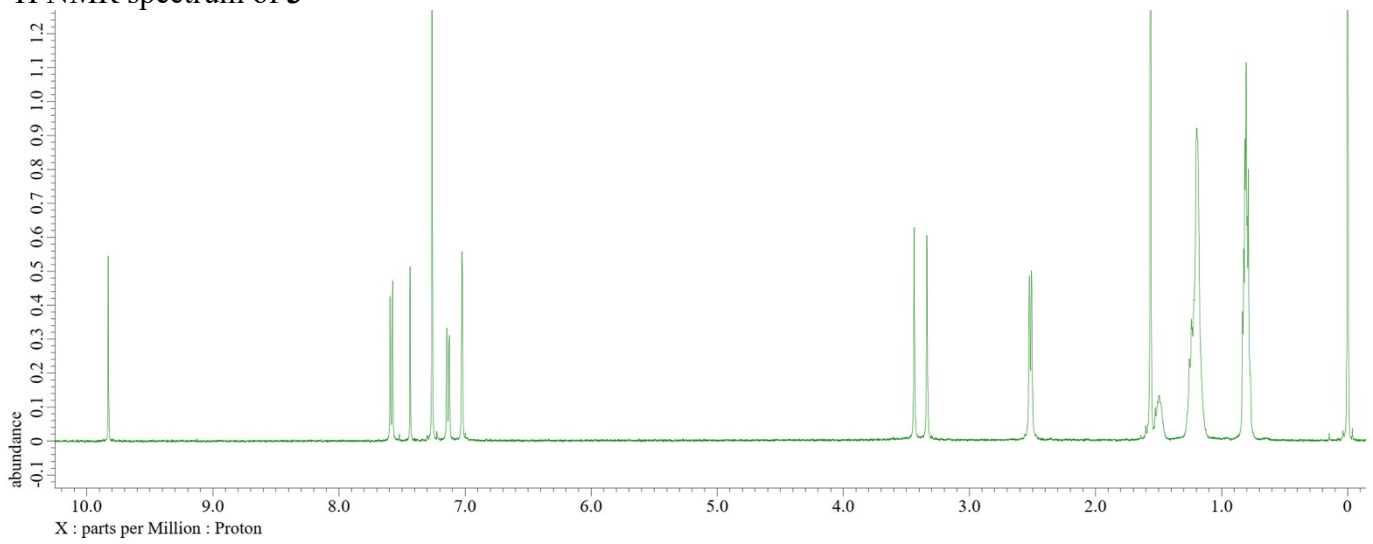

^{13}C NMR spectrum of **3**

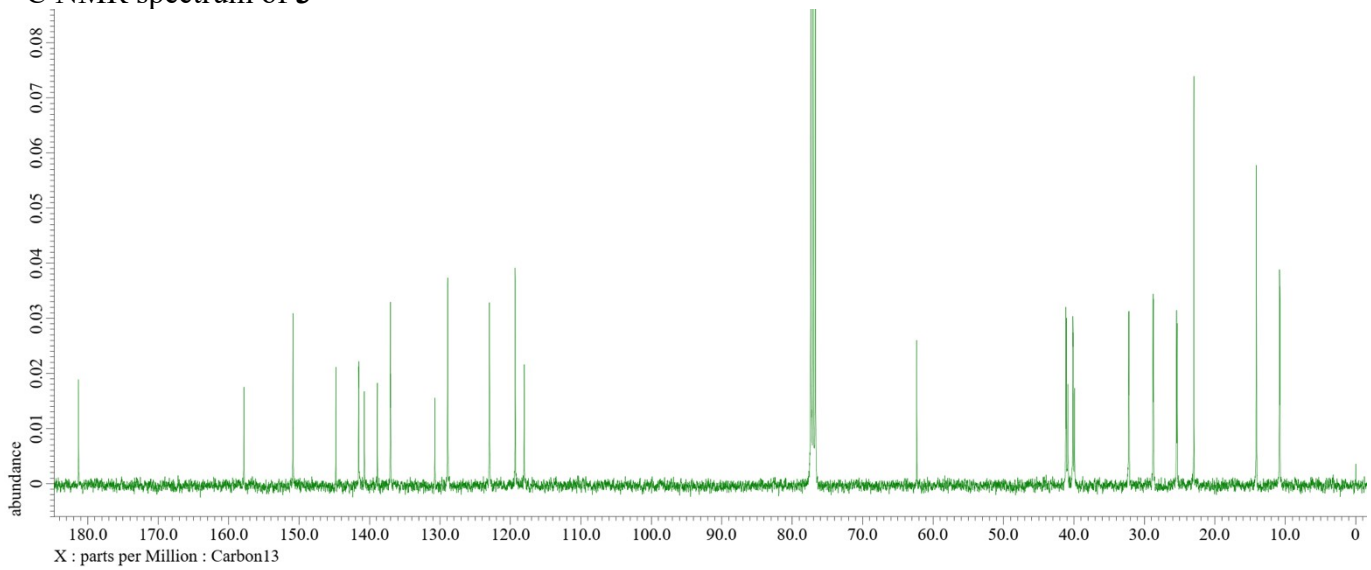

^{1}H NMR spectrum of **5**

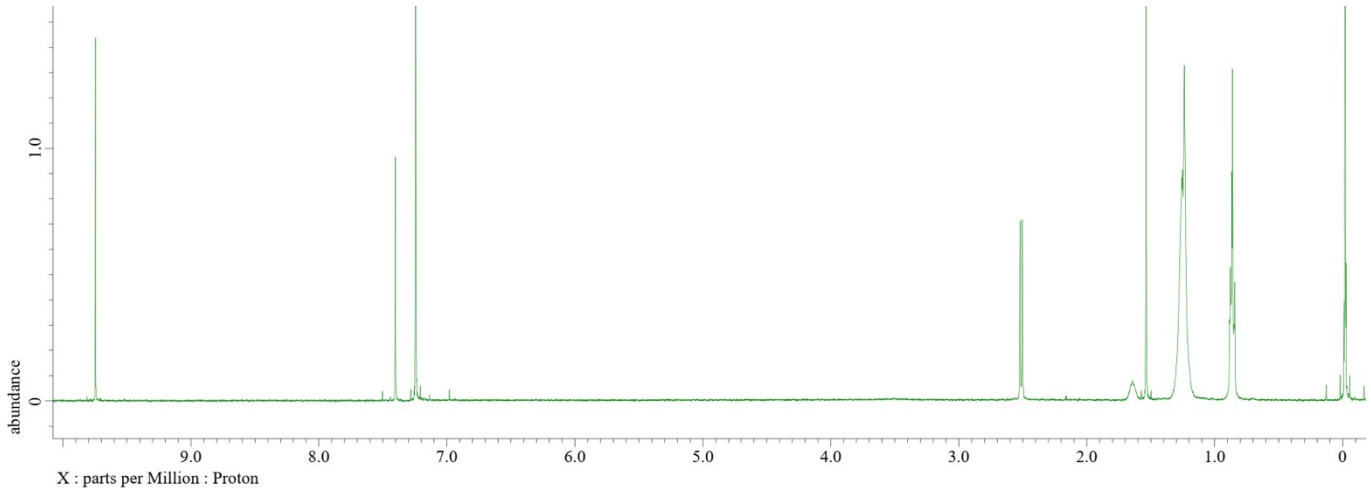

^{13}C NMR spectrum of **5**

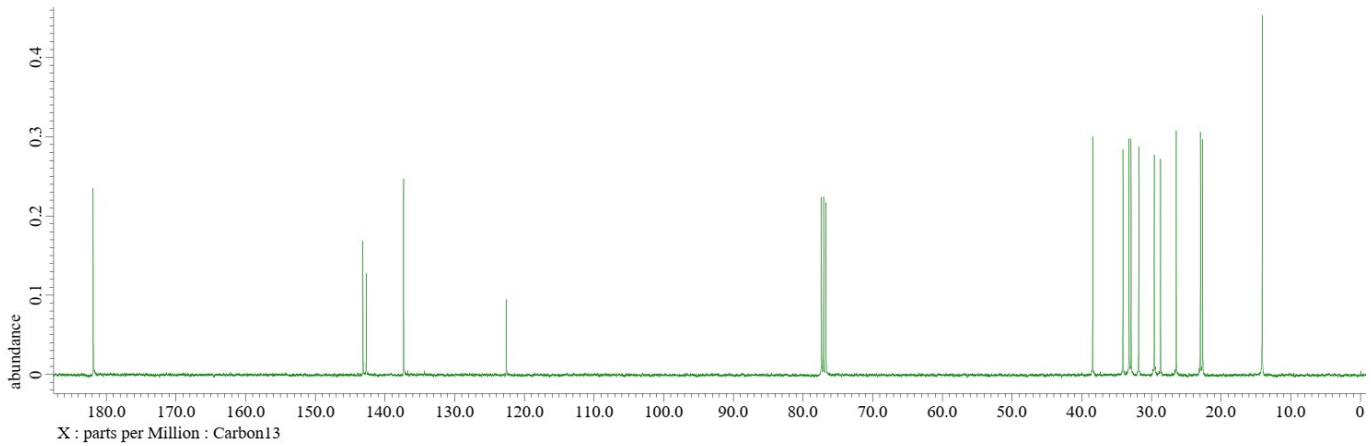

^{1}H NMR spectrum of **7**

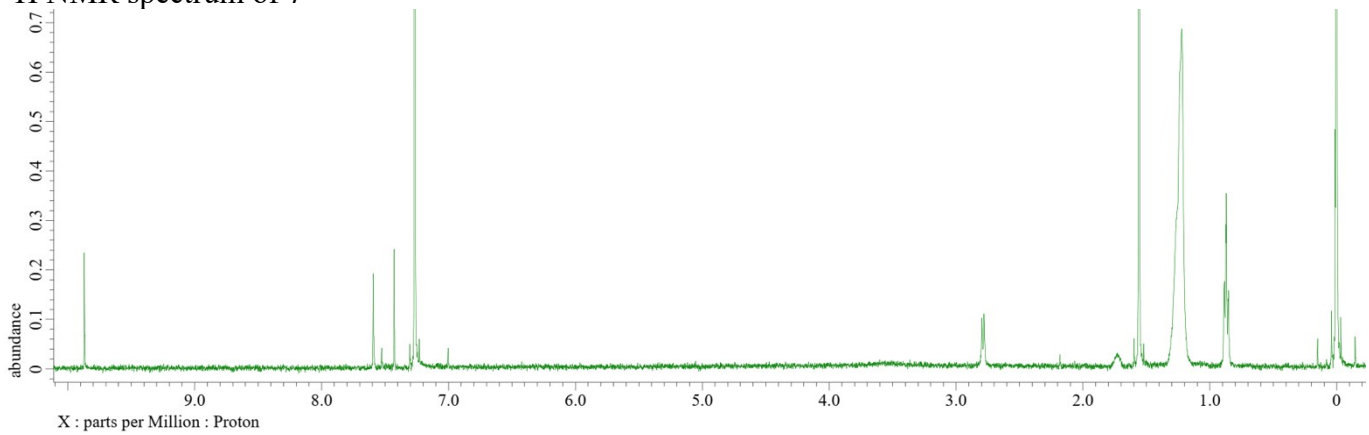

^{13}C NMR spectrum of **7**

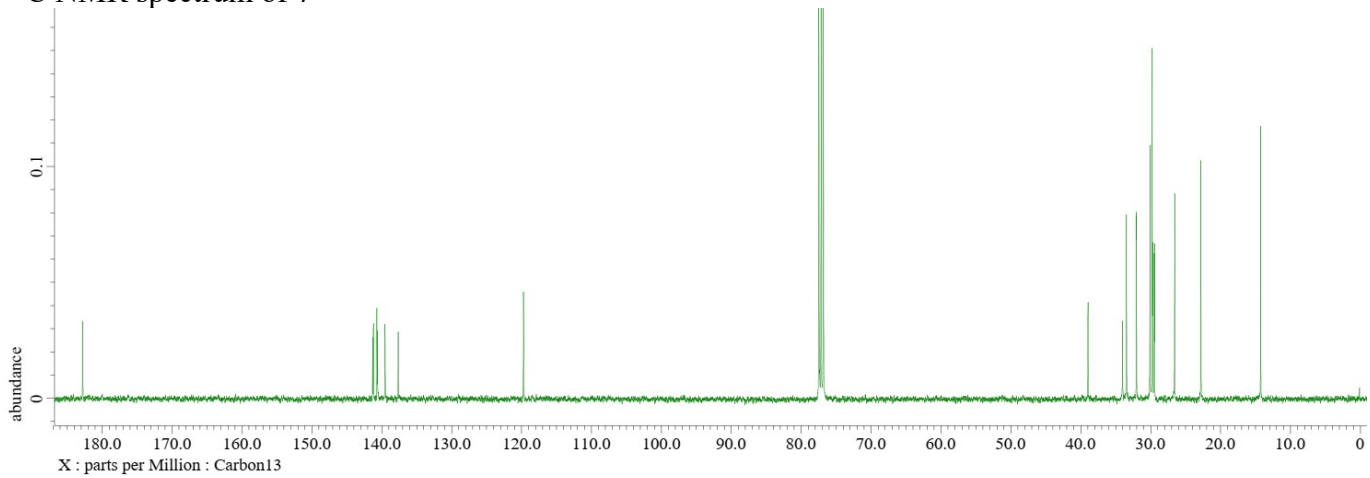

^{1}H NMR spectrum of **8**

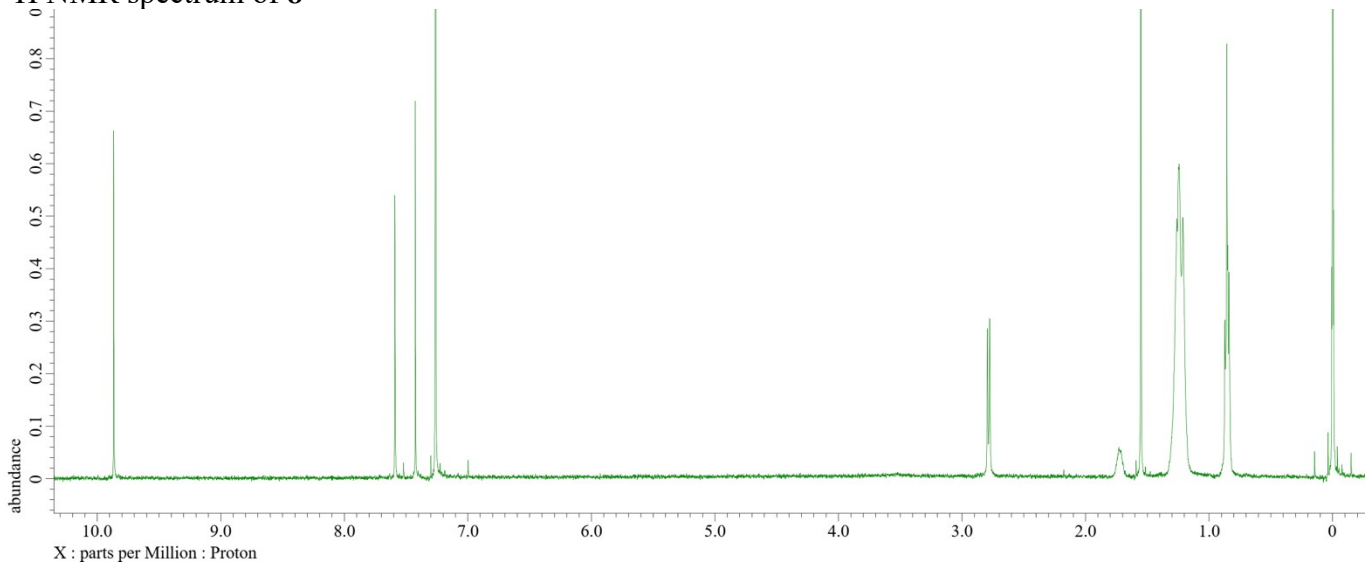

^{13}C NMR spectrum of **8**

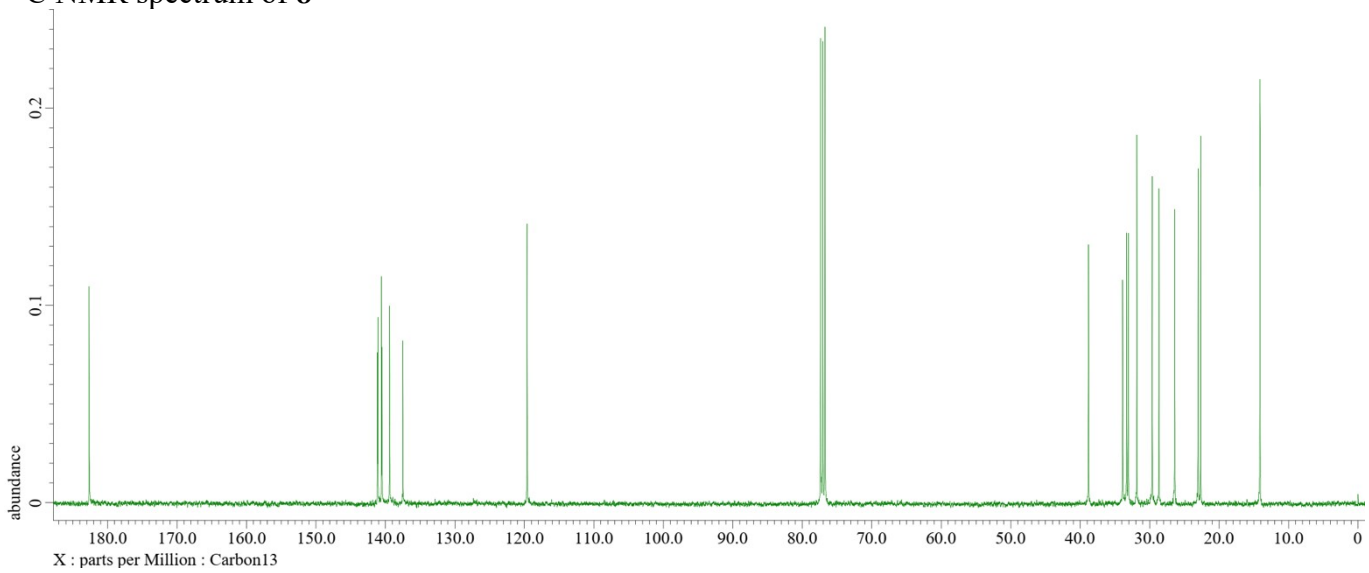

^{1}H NMR spectrum of **9**

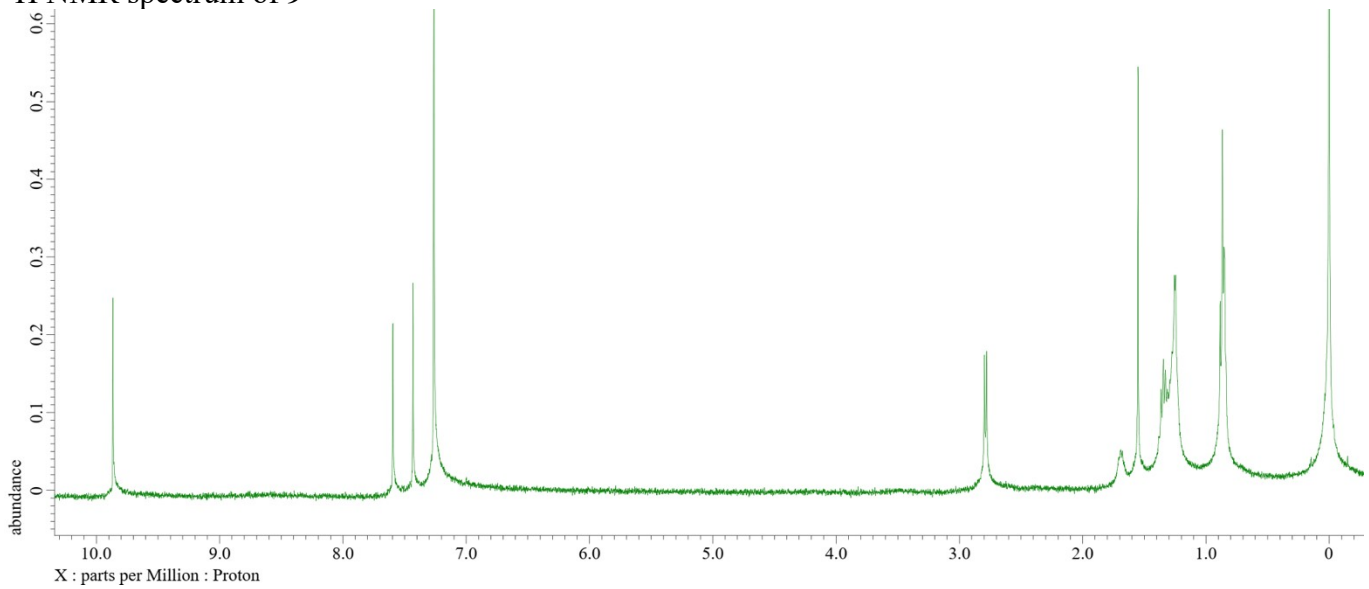

^{13}C NMR spectrum of **9**

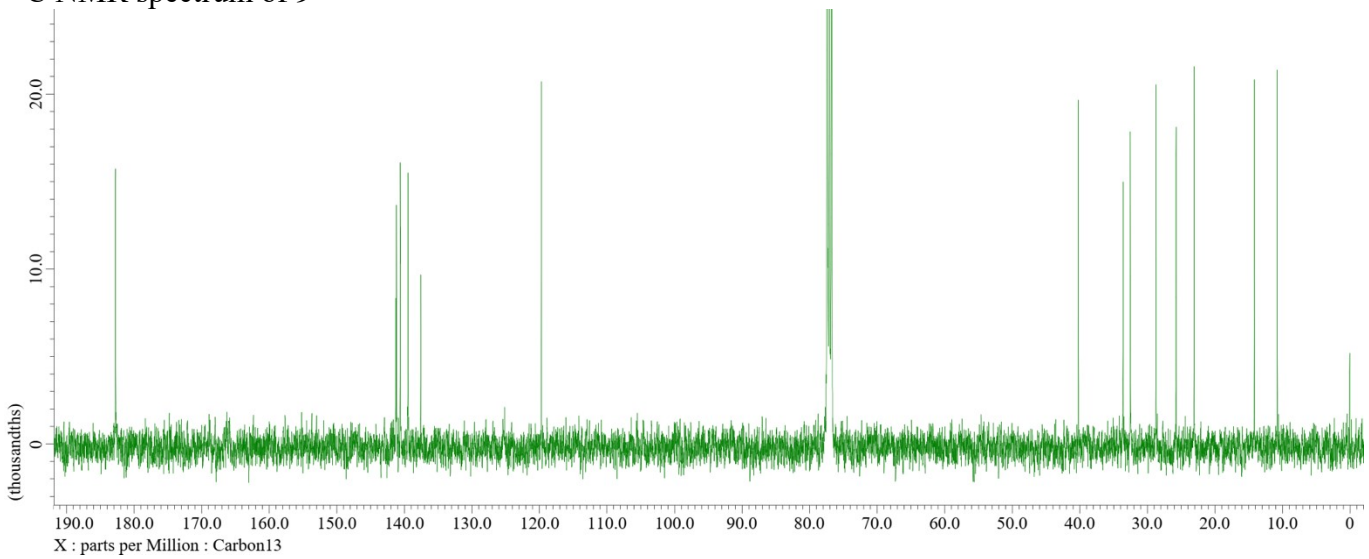

^{1}H NMR spectrum of **TT-FT-DCI**

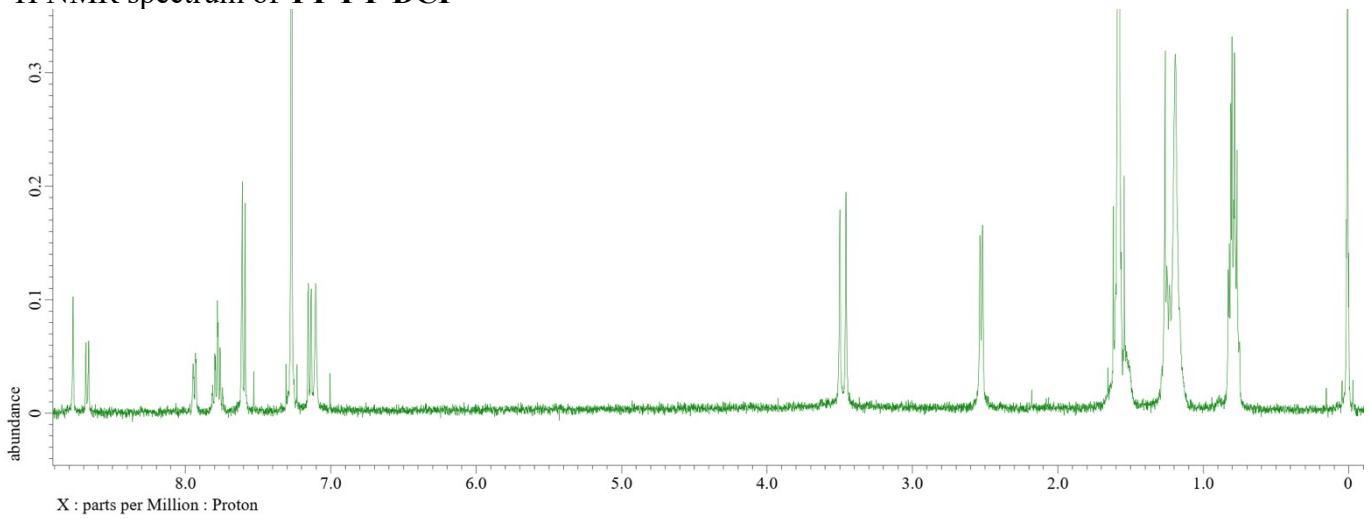

^{13}C NMR spectrum of **TT-FT-DCI**

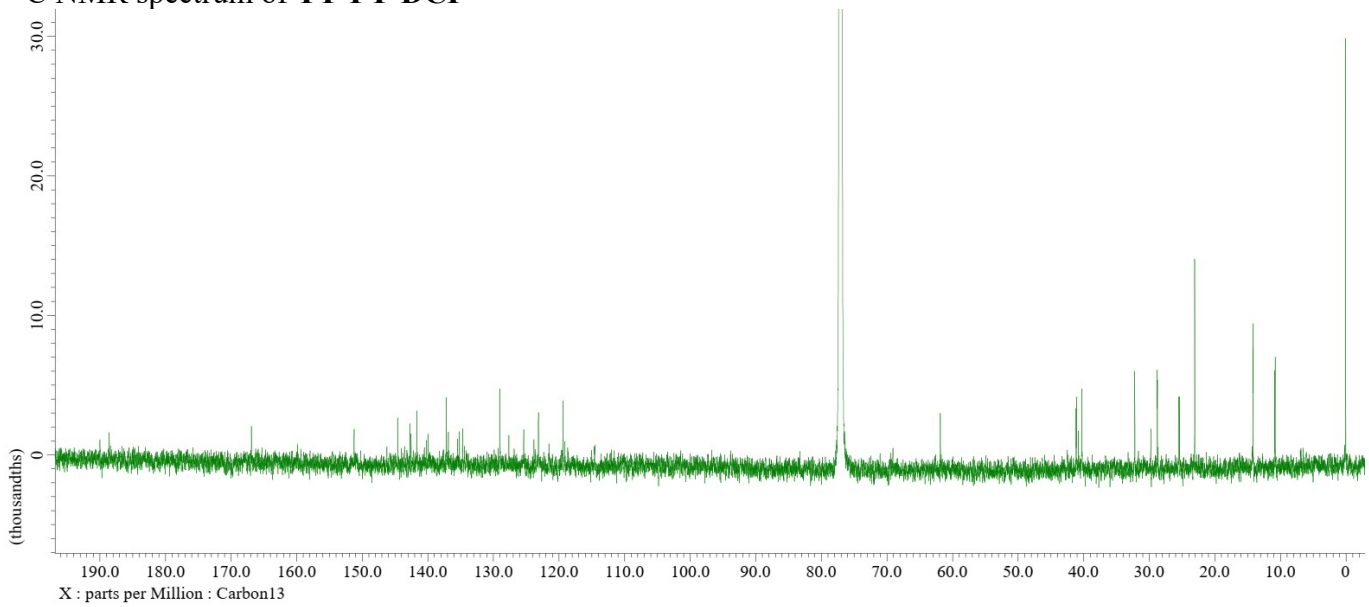

^{1}H NMR spectrum of **TT-T-DCI** (at 25°C)

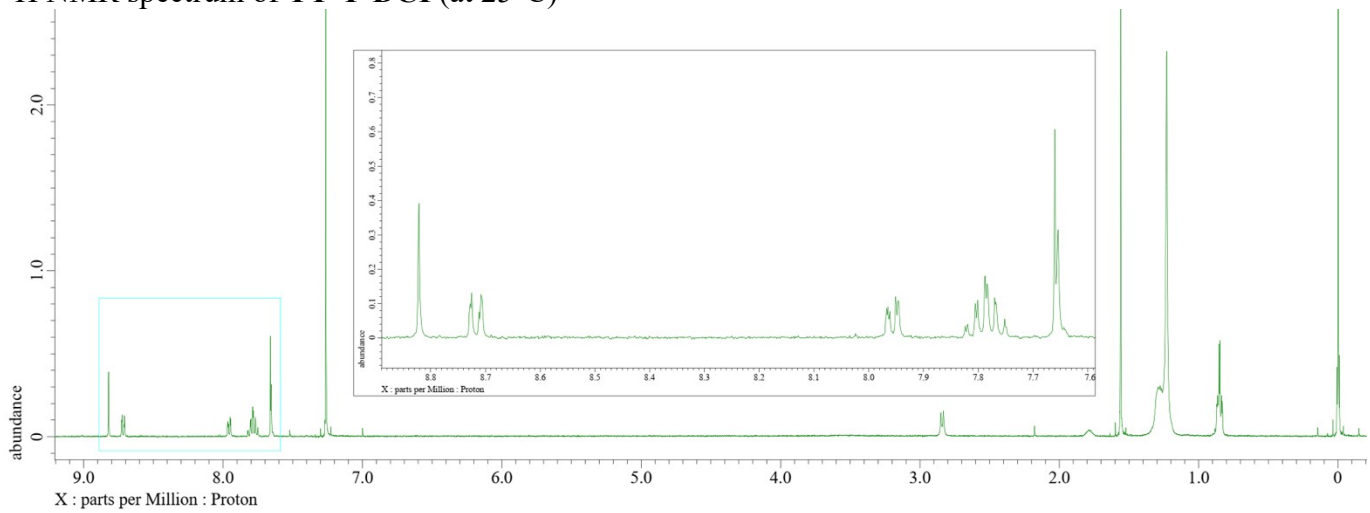

^{1}H NMR spectrum of **TT-T-DCI** (at 60°C)

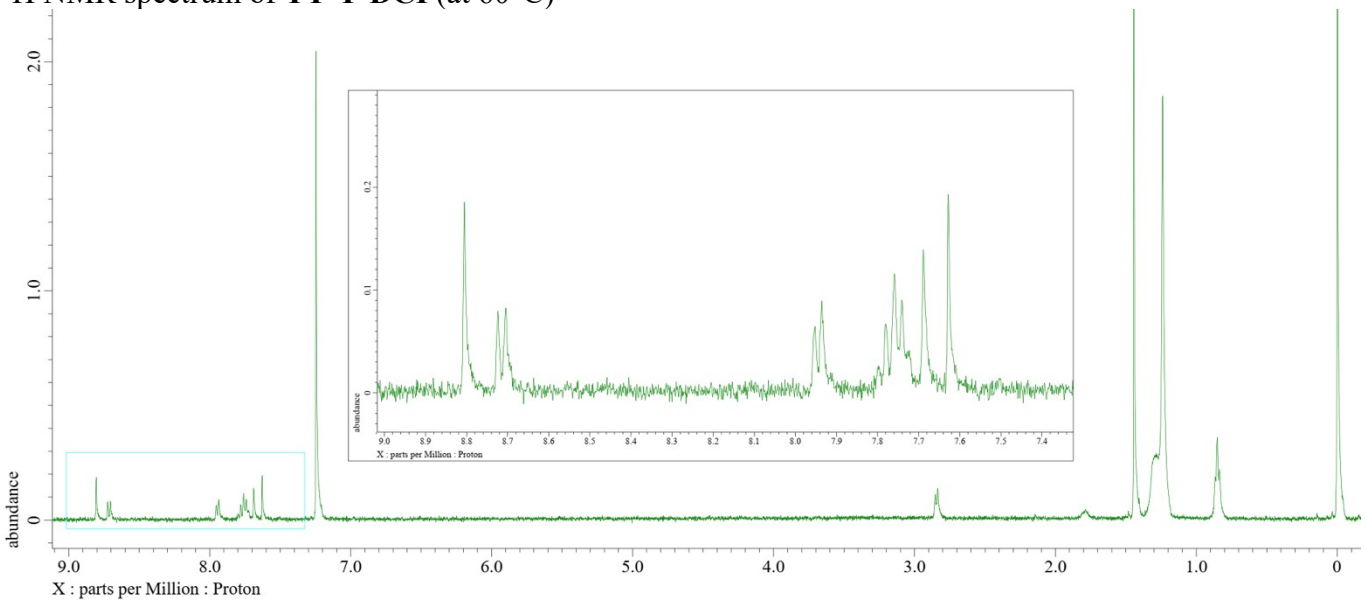

^{1}H NMR spectrum of **TT-T(bo)-DCI**

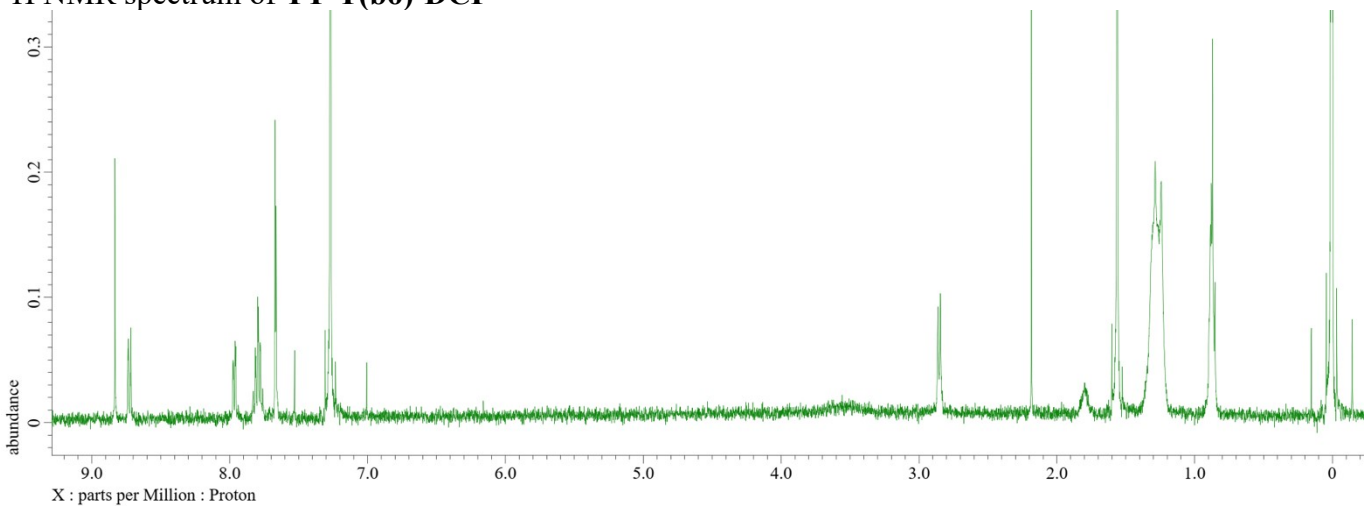

^{1}H NMR spectrum of **TT-T(eh)-DCI**

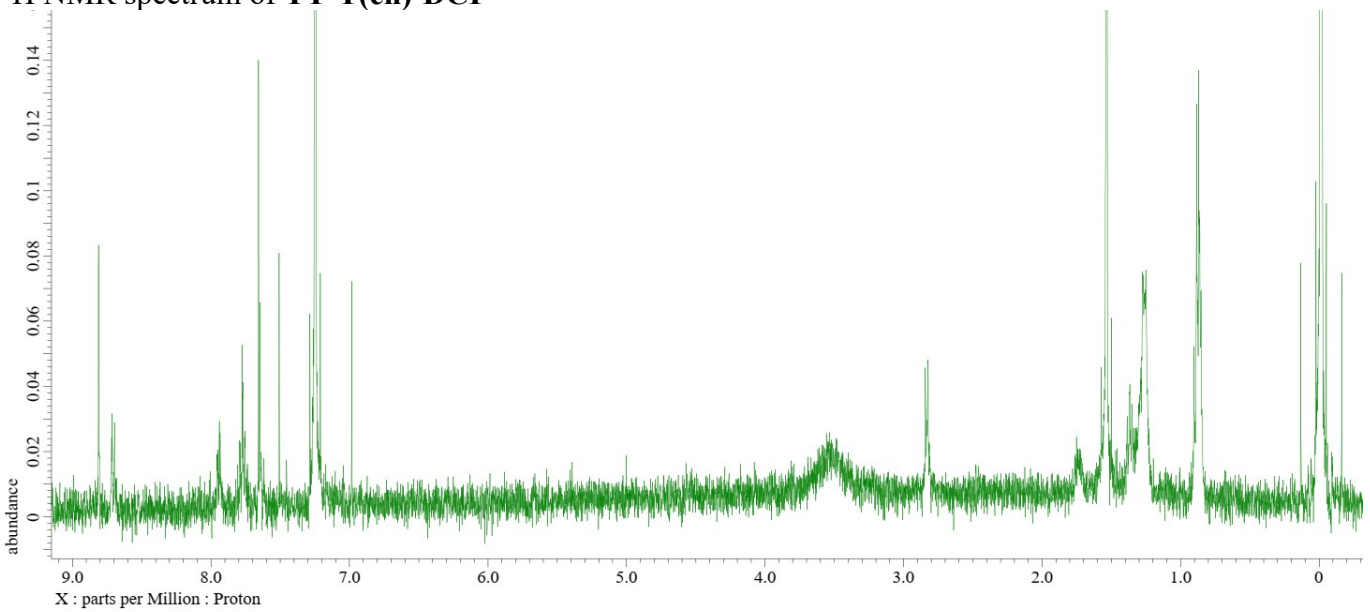

References

1 Y. Lin, J. Wang, Z. G. Zhang, H. Bai, Y. Li, D. Zhu and X. Zhan, *Adv. Mater.*, 2015, **27**, 1170–1174.

2 W. Zhao, D. Qian, S. Zhang, S. Li, O. Inganäs, F. Gao and J. Hou, *Adv. Mater.*, 2016, **28**, 4734–4739.

3 J. Yuan, Y. Zhang, L. Zhou, G. Zhang, H.-L. Yip, T.-K. Lau, X. Lu, C. Zhu, H. Peng, P. A. Johnson, M. Leclerc, Y. Cao, J. Ulanski, Y. Li and Y. Zou, *Joule*, 2019, **3**, 1140–1151.

4 L. Zhan, S. Li, Y. Li, R. Sun, J. Min, Z. Bi, W. Ma, Z. Chen, G. Zhou, H. Zhu, M. Shi, L. Zuo and H. Chen, *Joule*, 2022, **6**, 662–675.

5 D. Qian, L. Ye, M. Zhang, Y. Liang, L. Li, Y. Huang, X. Guo, S. Zhang, Z. Tan and J. Hou, *Macromolecules*, 2012, **45**, 9611–9617.

6 L.-M. Wang, Q. Li, S. Liu, Z. Cao, Y.-P. Cai, X. Jiao, H. Lai, W. Xie, X. Zhan and T. Zhu, *ACS Applied Materials & Interfaces*, 2020, **12**, 24165–24173.

7 M. Van Landeghem, W. Maes, E. Goovaerts and S. Van Doorslaer, *J. Magn. Reson.*, 2018, **288**, 1–10.

8 W. Zhao, S. Li, H. Yao, S. Zhang, Y. Zhang, B. Yang and J. Hou, *J. Am. Chem. Soc.*, 2017, **139**, 7148–7151.

9 S. D. Dimitrov and J. R. Durrant, *Chem. Mater.,* 2014, **26**, 616.

10 G. G. Malliaras, J. R. Salem, P. J. Brock and C. Scott, *Phys. Rev. B,* 1998, **58**, 13411

11 C. Goh, R. J. Kline, M. D. McGehee, E. N. Kadnikova and J. M. J. Fréchet, *Appl. Phys. Lett.,* 2005, **86**, 122110.

12 O. Gonen and H. Levanon, *J. Phys. Chem.*, 1984, **88**, 4223–4228.

13 M. Hasegawa, H. Nagashima, R. Minobe, T. Tachikawa, H. Mino and Y. Kobori, *J. Phys. Chem. Lett.*, 2017, **8**, 1179–1184.

14 P. J. Hore, D. A. Hunter, C. D. McKie and A. J. Hoff, *Chem. Phys. Lett.*, 1987, **137**, 495-500.

15 O. Gonen and H. Levanon, *J. Phys. Chem.*, 1984, **88**, 4223–4228.

16 T. Biskup, M. Sommer, S. Rein, D. L. Meyer, M. Kohlstadt, U. Wurfel and S. Weber, *Angew. Chem., Int. Ed.*, 2015, **54**, 7707–7710.

17 Y. Ie, Y. Okamoto, S. Tone and Y. Aso, *Chem. Eur. J.*, *2015*, **21**, 16688–16695.

18 Y. Zhou, M. Li, H. Lu, H. Jin, X. Wang, Y. Zhang, S. Shen, Z. Ma, J. Song and Z. Bo, *Adv. Funct. Mater.*, 2021, **31**, 2101742.

19 S. Cheng, S. H. Yu, S.-K. Kwon, D. S. Chung and Y.-H. Kim, *Dyes and Pigments*, 2019, **162**, 481–486.

Computational Details

Optimized geometry of TT-FT(m)-DCI and TT-T(m)-DCI (Fig. S3) was obtained by Gaussian 09 at B3LYP/6-31G(d,p) level.

Optimized structure of model compound for **TT-FT(m)-DCI**

Center Number	Atomic Number	Atomic Type	Coordinates (Angstroms) X	Y	Z
1	6	0	-0.034718	-0.659188	0.063640
2	6	0	0.034084	0.661423	-0.065106
3	6	0	1.314321	1.032995	-0.038925
4	6	0	2.091810	-0.062723	0.107896
5	16	0	1.271731	-1.294375	0.191955
6	6	0	-1.314893	-1.030874	0.037277
7	6	0	-2.092382	0.064844	-0.109544
8	16	0	-1.272276	1.296530	-0.193231
9	6	0	3.439765	-0.066797	0.176467
10	6	0	-3.440333	0.068969	-0.178201
11	6	0	-4.280549	1.101036	-0.315327
12	6	0	4.280005	-1.098713	0.314385
13	16	0	4.262414	1.154989	0.106910
14	6	0	5.636958	0.656434	0.238489
15	6	0	5.540014	-0.675883	0.352319
16	16	0	-4.263030	-1.152833	-0.109473
17	6	0	-5.637478	-0.654255	-0.241034
18	6	0	-5.540648	0.678118	-0.353785
19	6	0	-6.824670	-1.293476	-0.264778
20	6	0	-7.295482	-2.558891	-0.171145
21	6	0	6.824097	1.295586	0.261490
22	6	0	7.294929	2.560973	0.166674
23	6	0	-6.534316	1.791445	-0.501489
24	6	0	-5.624755	2.997136	-0.172304
25	6	0	-4.154426	2.590679	-0.427341
26	6	0	6.533699	-1.788994	0.501320
27	6	0	5.624239	-2.995536	0.174897
28	6	0	4.153695	-2.588339	0.427917
29	6	0	-6.047163	4.306439	-0.793988
30	6	0	-6.391061	5.236658	0.110057
31	6	0	-6.258826	4.728759	1.344123
32	6	0	-5.827062	3.460775	1.259388
33	6	0	5.827544	-3.464079	-1.255258
34	6	0	6.259148	-4.732653	-1.334520
35	6	0	6.390362	-5.236154	-0.098445
36	6	0	6.045952	-4.302549	0.801773
37	6	0	-6.098556	4.583059	-2.104347
38	6	0	-6.496680	5.799491	-2.520088
39	6	0	-6.838370	6.722239	-1.600472
40	6	0	-6.789759	6.453160	-0.285014
41	6	0	-6.487197	5.291948	2.538094
42	6	0	-6.275508	4.564299	3.647528
43	6	0	-5.842052	3.291055	3.580483
44	6	0	-5.618586	2.742441	2.372282
45	6	0	6.788558	-6.451216	0.301318
46	6	0	6.836024	-6.715512	1.617843
47	6	0	6.493789	-5.789347	2.533766
48	6	0	6.096295	-4.574363	2.113218
49	6	0	5.619845	-2.748532	-2.370372
50	6	0	5.844616	-3.302493	-3.575887
51	6	0	6.277852	-4.576044	-3.636942
52	6	0	6.488716	-5.300756	-2.525783
53	6	0	-5.603414	2.474639	4.828895
54	6	0	-6.552040	6.105293	-3.998419
55	6	0	5.618472	-2.520864	-4.848806
56	6	0	6.548128	-6.089646	4.013251
57	6	0	-6.530946	-3.674349	0.024058
58	6	0	-7.396064	-4.712432	0.056267
59	6	0	-8.647199	-4.272500	-0.109550
60	6	0	-8.608769	-2.928298	-0.254900
61	6	0	6.530495	3.676221	-0.029351
62	6	0	7.395630	4.714224	-0.062657
63	6	0	8.646732	4.274324	0.103294
64	6	0	8.608319	2.930338	0.249942
65	6	0	7.076986	6.005421	-0.236584
66	6	0	8.071975	6.905086	-0.243126
67	6	0	9.339319	6.495121	-0.078458
68	6	0	9.628169	5.193281	0.093486
69	6	0	-7.077402	-6.003708	0.229097
70	6	0	-8.072407	-6.903421	0.234676
71	6	0	-9.339688	-6.493402	0.070160
72	6	0	-9.628585	-5.191400	-0.100638
73	8	0	-5.339616	-3.837160	0.159935
74	8	0	5.339161	3.838980	-0.165142
75	6	0	9.709396	2.165994	0.443287
76	6	0	-9.709945	-2.163861	-0.447844
77	6	0	-9.757184	-0.853843	-0.606518
78	6	0	-10.946487	-2.624292	-0.514404
79	6	0	9.756714	0.856079	0.603076
80	6	0	10.946049	2.626486	0.509189
81	7	0	-12.048737	-2.980185	-0.579893
82	7	0	-9.828241	0.294967	-0.751127
83	7	0	9.827633	-0.292541	0.748727
84	7	0	12.048334	2.982231	0.574123
85	1	0	1.646087	2.077220	-0.126776
86	1	0	-1.646722	-2.075153	0.124976
87	1	0	-7.610985	-0.545796	-0.401201
88	1	0	7.610500	0.547994	0.398436
89	1	0	-7.410865	1.718029	0.178201
90	1	0	-6.871990	1.812572	-1.563032
91	1	0	-3.460811	3.057328	0.304773
92	1	0	-3.841901	2.834490	-1.468567
93	1	0	6.872287	-1.808079	1.562612
94	1	0	7.409806	-1.716620	-0.179131
95	1	0	3.839993	-2.830787	1.469208
96	1	0	3.460692	-3.055609	-0.304425
97	1	0	-5.814105	3.811473	-2.836908
98	1	0	-7.166614	7.723724	-1.924624
99	1	0	-7.075033	7.227261	0.444818
100	1	0	-6.841608	6.331372	2.622457
101	1	0	-6.463293	5.028632	4.629879
102	1	0	-5.263771	1.702886	2.298126
103	1	0	7.074225	-7.228099	-0.425381
104	1	0	7.163893	-7.715901	1.945903
105	1	0	5.811444	-3.800098	2.842816
106	1	0	5.265284	-1.709517	-2.292445
107	1	0	6.464221	-5.037311	-4.621251
108	1	0	6.842897	-6.340443	-2.606930
109	1	0	-5.815820	3.042961	5.761778
110	1	0	-6.256734	1.572419	4.829900
111	1	0	-4.541641	2.141148	4.874659
112	1	0	-7.264123	5.416802	-4.507903
113	1	0	-6.883397	7.146224	-4.210259
114	1	0	-5.545652	5.975075	-4.457713
115	1	0	6.565497	-2.448108	-5.430672
116	1	0	4.852824	-3.025603	-5.480931
117	1	0	5.263179	-1.483566	-4.657941
118	1	0	6.882168	-7.128912	4.229243
119	1	0	7.257582	-5.397357	4.521280
120	1	0	5.540617	-5.960628	4.470609
121	1	0	6.036631	6.341556	-0.371994
122	1	0	7.849426	7.976072	-0.383352
123	1	0	10.152965	7.240788	-0.085024
124	1	0	10.688043	4.944523	0.220545
125	1	0	-6.037019	-6.339926	0.364459
126	1	0	-7.849753	-7.974566	0.373994
127	1	0	-10.153262	-7.239197	0.075952
128	1	0	-10.688459	-4.942642	-0.227697

Optimized structure of model compound for **TT-T(m)-DCI**

Center	Atomic	Atomic	Coordinates (Angstroms)

Number	Number	Type	X	Y	Z
1	6	0	0.248538	0.616349	0.000091
2	6	0	-0.248530	-0.616435	0.000128
3	6	0	-1.580170	-0.547238	0.000151
4	6	0	-1.953607	0.751199	0.000093
5	16	0	-0.776752	1.654273	0.000074
6	6	0	1.580178	0.547152	0.000067
7	6	0	1.953597	-0.751210	0.000062
8	16	0	0.776762	-1.654294	0.000220
9	6	0	-3.223603	1.209798	0.000064
10	6	0	3.223594	-1.209809	0.000090
11	6	0	3.632122	-2.485794	0.000093
12	6	0	-3.632131	2.485783	0.000061
13	16	0	-4.407547	0.343943	0.000173
14	6	0	-5.504785	1.314037	0.000090
15	6	0	-4.968755	2.552333	0.000026
16	16	0	4.407540	-0.343888	0.000058
17	6	0	5.504775	-1.314048	0.000064
18	6	0	4.968844	-2.552332	0.000115
19	6	0	6.836124	-1.083410	0.000028
20	6	0	7.691795	-0.032603	-0.000005
21	6	0	-6.836136	1.083334	0.000050
22	6	0	-7.691824	0.032603	0.000019
23	6	0	7.336306	1.287436	0.000024
24	6	0	8.495365	1.983129	0.000039
25	6	0	9.534715	1.143366	-0.000111
26	6	0	9.056801	-0.121976	-0.000103
27	6	0	-7.336318	-1.287511	0.000054
28	6	0	-8.495394	-1.983130	-0.000024
29	6	0	-9.534685	-1.143335	-0.000167
30	6	0	-9.056867	0.122060	-0.000086
31	6	0	-8.617593	-3.319093	0.000003
32	6	0	-9.853596	-3.840197	-0.000106
33	6	0	-10.918196	-3.023134	-0.000163
34	6	0	-10.764276	-1.687545	-0.000189
35	6	0	8.617582	3.319018	0.000075
36	6	0	9.853547	3.840207	-0.000019
37	6	0	10.918226	3.023165	-0.000115
38	6	0	10.764304	1.687511	-0.000165
39	8	0	6.267277	1.855029	0.000176
40	8	0	-6.267362	-1.854996	0.000206
41	6	0	-9.853605	1.217542	-0.000132
42	6	0	9.853635	-1.217511	-0.000146
43	6	0	9.480432	-2.484127	-0.000204
44	6	0	11.174673	-1.192401	-0.000287
45	6	0	-9.480402	2.484158	-0.000074
46	6	0	-11.174683	1.192452	-0.000271
47	7	0	12.334441	-1.223634	-0.000366
48	7	0	9.183943	-3.605656	-0.000199
49	7	0	-9.184012	3.605675	-0.000066
50	7	0	-12.334354	1.223631	-0.000280
51	6	0	-5.704544	3.868482	-0.000043
52	6	0	5.704616	-3.868406	0.000120
53	1	0	-2.238268	-1.427668	0.000161
54	1	0	2.238259	1.427657	-0.000007
55	1	0	2.985338	-3.374486	0.000204
56	1	0	-2.985330	3.374400	0.000014
57	1	0	7.354971	-2.043967	0.000041
58	1	0	-7.355003	2.043902	-0.000102
59	1	0	-7.744078	-3.990452	0.000134
60	1	0	-9.993755	-4.934073	-0.000160
61	1	0	-11.932438	-3.458411	-0.000323
62	1	0	-11.686508	-1.095328	-0.000327
63	1	0	7.744089	3.990431	0.000160
64	1	0	9.993805	4.934093	0.000021
65	1	0	11.932445	3.458387	-0.000170
66	1	0	11.686499	1.095379	-0.000230
67	1	0	-5.004154	4.733425	0.000020
68	1	0	-6.338386	3.967840	-0.910172
69	1	0	-6.338602	3.967894	0.909963
70	1	0	5.004164	-4.733445	0.000274
71	1	0	6.338474	-3.967906	-0.909936
72	1	0	6.338554	-3.967818	0.910160

Optimized geometry of PBDB-T:TT-FT(m)-DCI model complex (Fig. 12) was obtained by Gaussian 16 at B3LYP/6-31G(d,p) level with empirical dispersion correction (GD3).

Optimized structure of PBDB-T:TT-FT(m)-DCI model complex.

Center Number	Atomic Number	Atomic Type	Coordinates (Angstroms) X	Y	Z
1	6	0	-6.334634	2.672678	-0.649312
2	6	0	-7.740439	2.449760	-0.854624
3	16	0	-8.694616	1.627622	0.373503
4	6	0	-10.184972	1.824677	-0.565720
5	6	0	-9.888972	2.501245	-1.756022
6	6	0	-8.541830	2.838922	-1.926686
7	6	0	-10.729355	3.006920	-2.897232
8	6	0	-9.674314	3.354062	-4.010240
9	6	0	-8.325416	3.575776	-3.223691
10	6	0	-11.503407	1.393148	-0.273727
11	6	0	-10.060327	4.542034	-4.884096
12	6	0	-10.130231	4.164815	-6.238083
13	6	0	-9.820234	2.734212	-6.340565
14	6	0	-9.556077	2.235526	-5.048936
15	6	0	-10.315159	5.852712	-4.501947
16	6	0	-10.649629	6.816764	-5.468092
17	6	0	-10.710240	6.426564	-6.814497
18	6	0	-10.455460	5.111997	-7.208942
19	6	0	-9.768348	1.881978	-7.442233
20	6	0	-9.462024	0.534591	-7.242309
21	6	0	-9.208983	0.019615	-5.962824
22	6	0	-9.253127	0.892911	-4.860906
23	6	0	-12.087348	0.738337	0.790163
24	6	0	-11.401480	0.347310	2.044333
25	6	0	-12.436639	-0.226549	2.933583
26	6	0	-13.680773	-0.212277	2.276161
27	6	0	-13.498150	0.360248	0.915995
28	6	0	-12.277413	-0.716640	4.222187
29	6	0	-13.405400	-1.209478	4.880824
30	6	0	-14.651282	-1.200512	4.242250
31	6	0	-14.807351	-0.707947	2.942917
32	8	0	-10.213981	0.478773	2.316253
33	6	0	-14.500133	0.465230	-0.034921
34	6	0	-8.931025	-1.451473	-5.764618
35	6	0	-10.964289	8.236746	-5.059890
36	16	0	-5.397382	3.632283	-1.817083
37	6	0	-3.964652	3.472488	-0.844725
38	6	0	-4.218035	2.714983	0.305158
39	6	0	-5.548126	2.260331	0.417859
40	16	0	-2.783164	2.587626	1.288162
41	6	0	-2.646959	3.953995	-0.948696
42	6	0	-1.863346	3.573881	0.131404
43	6	0	-0.484518	3.918471	0.355083
44	16	0	0.416521	4.696093	-0.944732
45	6	0	1.855696	4.866821	0.072050
46	6	0	1.590857	4.312147	1.329296
47	6	0	0.306043	3.776196	1.493091
48	6	0	2.409550	4.157946	2.577596
49	6	0	1.335961	3.834121	3.680444
50	6	0	0.135521	3.200610	2.879747
51	6	0	3.108178	5.462841	-0.219873
52	6	0	1.908997	2.975354	4.801448
53	6	0	1.870587	3.666790	6.027998
54	6	0	1.237773	4.972569	5.809084
55	6	0	0.913517	5.092783	4.443213
56	6	0	0.939982	6.009592	6.692374
57	6	0	0.319971	7.160164	6.202224
58	6	0	-0.006936	7.296917	4.845275
59	6	0	0.296059	6.242532	3.966134
60	6	0	2.470848	1.707701	4.720669
61	6	0	3.025779	1.108334	5.864979
62	6	0	2.981748	1.810396	7.079956
63	6	0	2.406187	3.079947	7.174741
64	6	0	3.647658	6.067217	-1.335929
65	6	0	4.984352	6.657986	-1.449781
66	6	0	5.137822	7.132811	-2.851192
67	6	0	3.946058	6.871488	-3.552263
68	6	0	2.976393	6.212818	-2.648608
69	6	0	6.199242	7.750070	-3.523433
70	6	0	6.031914	8.085679	-4.870646
71	6	0	4.838010	7.820959	-5.552139
72	6	0	3.775557	7.204560	-4.888731
73	6	0	5.948418	6.794259	-0.464564
74	8	0	1.841673	5.859642	-2.949615
75	6	0	3.693804	-0.243479	5.774012
76	6	0	-0.649255	8.562850	4.328490
77	7	0	8.269313	7.895906	-0.821642
78	7	0	5.689422	6.024194	1.998673
79	6	0	7.221549	7.404486	-0.686769
80	6	0	-15.855814	0.080134	0.201383
81	6	0	5.784530	6.359590	0.886344
82	6	0	-14.291458	0.946412	-1.363821
83	7	0	-16.973022	-0.214071	0.352508
84	7	0	-14.149178	1.324140	-2.457788
85	1	0	-11.269770	3.911715	-2.589705
86	1	0	-11.481097	2.299176	-3.257011
87	1	0	-7.471674	3.213570	-3.803464
88	1	0	-8.158543	4.645170	-3.042265
89	1	0	-12.171812	1.660098	-1.083738
90	1	0	-10.258700	6.146664	-3.455298
91	1	0	-10.962151	7.169065	-7.567443
92	1	0	-10.508798	4.838882	-8.259116
93	1	0	-9.964616	2.253317	-8.444284
94	1	0	-9.423057	-0.135556	-8.097248
95	1	0	-9.056282	0.502745	-3.864952
96	1	0	-11.296213	-0.707283	4.685894
97	1	0	-13.320581	-1.601179	5.889830
98	1	0	-15.521695	-1.585699	4.764459
99	1	0	-15.786790	-0.719311	2.485296
100	1	0	-8.641684	-1.934066	-6.702492
101	1	0	-8.126241	-1.619011	-5.040219
102	1	0	-9.817969	-1.971927	-5.383453
103	1	0	-10.364114	8.549543	-4.199754
104	1	0	-10.775732	8.939350	-5.876747
105	1	0	-12.018522	8.344390	-4.774773
106	1	0	-5.931762	1.664053	1.236832
107	1	0	-2.276705	4.572302	-1.757095
108	1	0	3.008294	5.035130	2.838032
109	1	0	3.107731	3.318093	2.468401
110	1	0	0.218002	2.106160	2.860837
111	1	0	-0.822308	3.444458	3.347890
112	1	0	3.757824	5.411643	0.645774
113	1	0	1.178452	5.927690	7.749206
114	1	0	0.081864	7.970154	6.886958
115	1	0	0.039689	6.338303	2.913910
116	1	0	2.486724	1.167763	3.776785
117	1	0	3.411519	1.353316	7.967821
118	1	0	2.386576	3.599289	8.128884
119	1	0	7.137975	7.970895	-3.034841
120	1	0	6.852593	8.563343	-5.397013
121	1	0	4.742511	8.095846	-6.598093
122	1	0	2.836319	6.982636	-5.385112
123	1	0	3.743940	-0.732138	6.751497
124	1	0	3.161966	-0.910142	5.087758
125	1	0	4.721366	-0.145664	5.402637
126	1	0	0.101060	9.250924	3.918780

127	1	0	-1.363883	8.351411	3.526872
128	1	0	-1.179892	9.095801	5.122692
129	6	0	-11.084103	-4.013868	-1.263775
130	6	0	-10.612500	-4.712204	-0.113319
131	6	0	-11.424947	-5.691062	0.511031
132	6	0	-12.677290	-5.922637	-0.073766
133	6	0	-13.148021	-5.220478	-1.222864
134	6	0	-12.334805	-4.242651	-1.846343
135	6	0	-8.731867	-3.386922	-0.599918
136	6	0	-9.272123	-4.334839	0.226787
137	6	0	-15.007842	-6.545480	-0.739278
138	6	0	-14.492779	-5.604863	-1.569495
139	16	0	-13.908202	-7.034274	0.527501
140	16	0	-9.867790	-2.887431	-1.863074
141	6	0	-7.406882	-2.810684	-0.547418
142	6	0	-6.712118	-2.170886	-1.561939
143	16	0	-6.484284	-2.833197	0.933391
144	6	0	-5.429008	-1.758194	-1.168744
145	6	0	-5.109242	-2.053812	0.155185
146	6	0	-3.800543	-1.840484	0.732831
147	6	0	-3.288760	-1.727047	2.024098
148	16	0	-2.486322	-1.661716	-0.418668
149	6	0	-1.877771	-1.431602	2.075175
150	6	0	-4.074920	-1.892102	3.250580
151	6	0	-1.264861	-1.374980	0.820063
152	6	0	-1.215474	-1.169061	3.358619
153	6	0	-3.381100	-1.626092	4.534629
154	8	0	-5.252801	-2.261086	3.216139
155	6	0	-2.043848	-1.306018	4.587670
156	8	0	-0.028064	-0.827091	3.413697
157	6	0	-4.045775	-1.708908	5.835056
158	6	0	-1.520280	-1.121040	5.941124
159	16	0	-2.845017	-1.380911	7.122922
160	6	0	0.086369	-1.216248	0.329306
161	6	0	0.425138	-1.293637	-1.020751
162	16	0	1.559929	-1.030140	1.287379
163	6	0	1.798770	-1.222025	-1.287383
164	6	0	2.565270	-1.077926	-0.142616
165	6	0	-10.955680	-6.398032	1.713872
166	6	0	-10.474554	-5.852760	2.879762
167	16	0	-10.894622	-8.154115	1.807573
168	6	0	-10.069485	-6.822612	3.842106
169	6	0	-10.230428	-8.116686	3.422655
170	6	0	-9.916907	-9.382012	4.163436
171	6	0	-12.766523	-3.484031	-3.032696
172	6	0	-12.802586	-2.120859	-3.195080
173	16	0	-13.271616	-4.275000	-4.521127
174	6	0	-13.241403	-1.705012	-4.486206
175	6	0	-13.536187	-2.744675	-5.327356
176	6	0	-14.030986	-2.686818	-6.741463
177	6	0	-5.344168	-1.973421	6.094670
178	6	0	-5.963492	-2.030174	7.455045
179	6	0	-0.262587	-0.815752	6.323068
180	6	0	0.197234	-0.659267	7.737010
181	6	0	4.007793	-1.000298	-0.068840
182	6	0	4.803394	-0.430516	0.889872
183	16	0	4.963413	-1.743604	-1.360747
184	6	0	6.207813	-0.545876	0.626346
185	6	0	6.465829	-1.256023	-0.584833
186	6	0	7.284682	-0.079683	1.423212
187	6	0	7.752150	-1.568100	-1.038264
188	6	0	8.569860	-0.397644	0.972947
189	6	0	7.087286	0.720094	2.643275
190	6	0	8.827584	-1.122453	-0.228615
191	6	0	8.005685	-2.325846	-2.274862
192	16	0	10.072876	0.084965	1.754586
193	6	0	7.600762	0.505588	3.899816
194	16	0	6.220999	2.249719	2.605765
195	6	0	10.229887	-1.244148	-0.488064
196	6	0	8.752697	-3.468799	-2.426528
197	16	0	7.387489	-1.805702	-3.838161
198	6	0	11.026703	-0.658937	0.460919
199	6	0	7.291639	1.543471	4.827773
200	6	0	6.548466	2.563827	4.293047
201	6	0	8.824578	-3.932464	-3.772131
202	6	0	8.140322	-3.149000	-4.663198
203	6	0	12.469441	-0.592494	0.498825
204	6	0	6.028502	3.798039	4.966924
205	6	0	7.996065	-3.330490	-6.144454
206	6	0	13.263558	0.208991	1.303644
207	16	0	13.443085	-1.626948	-0.518650
208	6	0	14.635509	0.019127	1.079908
209	6	0	14.937219	-0.931433	0.106269
210	6	0	16.279791	-1.219571	-0.347034
211	6	0	16.886913	-2.239973	-1.079210
212	16	0	17.507164	-0.045232	0.115221
213	6	0	18.314334	-2.092110	-1.218639
214	6	0	16.193477	-3.403124	-1.645357
215	6	0	18.831192	-0.960468	-0.592193
216	6	0	19.107260	-3.094208	-1.943445
217	6	0	17.046116	-4.488263	-2.199351
218	8	0	14.961638	-3.479693	-1.658826
219	6	0	20.154400	-0.404781	-0.385343
220	6	0	18.405837	-4.344608	-2.338108
221	8	0	20.296136	-2.907024	-2.213770
222	6	0	16.517250	-5.771582	-2.662196
223	6	0	20.446633	0.565373	0.568153
224	16	0	21.599962	-0.750146	-1.332571
225	6	0	19.086000	-5.498473	-2.925893
226	16	0	17.875798	-6.779937	-3.257723
227	6	0	15.235941	-6.195730	-2.658174
228	6	0	21.779484	1.030236	0.533558
229	6	0	22.511685	0.418410	-0.453072
230	6	0	20.401457	-5.644894	-3.190406
231	6	0	14.758790	-7.531037	-3.134012
232	6	0	21.041155	-6.859444	-3.783962
233	1	0	-8.720539	-4.790732	1.039049
234	1	0	-15.990148	-6.996032	-0.785575
235	1	0	-15.039526	-5.178238	-2.399882
236	1	0	-7.115607	-2.021737	-2.556840
237	1	0	-4.744389	-1.246326	-1.835179
238	1	0	-0.311275	-1.409852	-1.807131
239	1	0	2.220569	-1.253258	-2.285181
240	1	0	-10.432420	-4.782426	3.046813
241	1	0	-9.674889	-6.569732	4.820431
242	1	0	-9.177537	-9.993966	3.634703
243	1	0	-9.508489	-9.140451	5.148509
244	1	0	-10.808979	-10.000884	4.311595
245	1	0	-12.545229	-1.430408	-2.401117
246	1	0	-13.353585	-0.664042	-4.768257
247	1	0	-13.351060	-3.193368	-7.435813
248	1	0	-15.016708	-3.153464	-6.849164
249	1	0	-14.117222	-1.643620	-7.056899
250	1	0	-5.983141	-2.165707	5.241507
251	1	0	-6.325364	-3.043640	7.674837
252	1	0	-6.838738	-1.370523	7.507989
253	1	0	-5.273487	-1.740796	8.252017
254	1	0	0.466407	-0.664186	5.537099
255	1	0	1.000175	-1.374047	7.960768
256	1	0	0.620675	0.340226	7.892168
257	1	0	-0.602113	-0.812591	8.466672
258	1	0	4.406197	0.076123	1.760257
259	1	0	8.176586	-0.377265	4.153349
260	1	0	10.623888	-1.724649	-1.374487
261	1	0	9.221045	-3.973075	-1.588929
262	1	0	7.611926	1.536849	5.864132
263	1	0	9.363282	-4.825049	-4.071584
264	1	0	6.171813	4.688508	4.348103

265	1	0	4.957732	3.713454	5.185015
266	1	0	6.551197	3.946099	5.916131
267	1	0	6.948620	-3.455197	-6.441159
268	1	0	8.542978	-4.222791	-6.460807
269	1	0	8.395902	-2.476597	-6.702672
270	1	0	12.864904	0.915873	2.022137
271	1	0	15.398840	0.560435	1.626370
272	1	0	19.716923	0.916721	1.288315
273	1	0	14.495329	-5.502147	-2.278399
274	1	0	22.178092	1.773607	1.213682
275	1	0	23.556283	0.568395	-0.692288
276	1	0	21.041875	-4.803919	-2.952648
277	1	0	14.006042	-7.413507	-3.924237
278	1	0	14.268757	-8.079767	-2.319027
279	1	0	15.563453	-8.158659	-3.525691
280	1	0	21.584527	-6.599992	-4.701594
281	1	0	21.783531	-7.281866	-3.094076
282	1	0	20.322535	-7.646188	-4.027822

The Cartesian coordinates of the optimized geometries of **TT-FT(m)-DCI in the triplet state**

CARTESIAN COORDINATES (A.U.)

NO	LB	ZA	FRAG	MASS	X	Y	Z
0	C	6.0000	0	12.011	0.220644	1.302116	-0.174422
1	C	6.0000	0	12.011	-0.221136	-1.298639	0.162271
2	C	6.0000	0	12.011	-2.798080	-1.972439	0.111003
3	C	6.0000	0	12.011	-4.360959	0.104237	-0.262218
4	S	16.0000	0	32.060	-2.593479	2.941359	-0.560020
5	C	6.0000	0	12.011	2.797551	1.975935	-0.122964
6	C	6.0000	0	12.011	4.360467	-0.100609	0.250899
7	S	16.0000	0	32.060	2.592988	-2.937768	0.548606
8	C	6.0000	0	12.011	-7.067084	0.115443	-0.431141
9	S	16.0000	0	32.060	-8.767252	-2.744090	-0.341927
10	C	6.0000	0	12.011	-11.691225	-1.132267	-0.638028
11	C	6.0000	0	12.011	-11.242491	1.471114	-0.810012
12	C	6.0000	0	12.011	-8.687751	2.173355	-0.679942
13	C	6.0000	0	12.011	-14.188291	-2.101186	-0.656925
14	C	6.0000	0	12.011	-15.161594	-4.499967	-0.497130
15	C	6.0000	0	12.011	-13.640988	-6.837728	-0.330853
16	C	6.0000	0	12.011	-15.451213	-8.968867	-0.280794
17	C	6.0000	0	12.011	-17.943743	-8.036212	-0.385183
18	C	6.0000	0	12.011	-17.849465	-5.213962	-0.494107
19	C	6.0000	0	12.011	-14.907029	-11.525440	-0.154655
20	C	6.0000	0	12.011	-16.926088	-13.229803	-0.134416
21	C	6.0000	0	12.011	-19.414234	-12.336378	-0.239882
22	C	6.0000	0	12.011	-19.956207	-9.747831	-0.364509
23	C	6.0000	0	12.011	-19.932283	-3.649704	-0.533621
24	C	6.0000	0	12.011	-22.452176	-4.581679	-0.515801
25	C	6.0000	0	12.011	-19.766535	-0.967653	-0.576423
26	N	7.0000	0	14.007	-24.531480	-5.321261	-0.505067
27	N	7.0000	0	14.007	-19.636749	1.236542	-0.608813
28	O	8.0000	0	15.999	-11.296254	-7.007105	-0.255585
29	C	6.0000	0	12.011	-12.934287	3.751258	-1.157533
30	C	6.0000	0	12.011	-11.159022	6.003509	-0.350393
31	C	6.0000	0	12.011	-8.383713	5.017242	-0.848241
32	C	6.0000	0	12.011	-11.756610	8.506546	-1.658386
33	C	6.0000	0	12.011	-11.529011	6.685246	2.444134
34	C	6.0000	0	12.011	-12.227964	9.252099	2.684828
35	C	6.0000	0	12.011	-12.370922	10.380096	0.142353
36	C	6.0000	0	12.011	-11.746160	9.064582	-4.218095
37	C	6.0000	0	12.011	-12.355124	11.521509	-5.038161
38	C	6.0000	0	12.011	-12.958173	13.366127	-3.234172
39	C	6.0000	0	12.011	-12.972592	12.817483	-0.648271
40	C	6.0000	0	12.011	-12.650242	10.288312	5.066866
41	C	6.0000	0	12.011	-12.373813	8.750623	7.199157
42	C	6.0000	0	12.011	-11.687314	6.201193	6.983634
43	C	6.0000	0	12.011	-11.261350	5.172124	4.566844
44	C	6.0000	0	12.011	-11.422903	4.545377	9.313062
45	C	6.0000	0	12.011	7.066536	-0.111399	0.420332
46	S	16.0000	0	32.060	8.767139	2.747284	0.315528
47	C	6.0000	0	12.011	11.690677	1.136935	0.623232
48	C	6.0000	0	12.011	11.241508	-1.465426	0.809578
49	C	6.0000	0	12.011	8.686882	-2.168158	0.681303
50	C	6.0000	0	12.011	12.932870	-3.743340	1.172821
51	C	6.0000	0	12.011	11.158266	-6.000901	0.379287
52	C	6.0000	0	12.011	8.382277	-5.010892	0.866931
53	C	6.0000	0	12.011	11.531619	-6.702594	-2.409703
54	C	6.0000	0	12.011	11.754304	-8.494508	1.705856
55	C	6.0000	0	12.011	12.371848	-10.380738	-0.080842

56 C	6.0000	0	12.011	12.232027	-9.270505	-2.631330
57 C	6.0000	0	12.011	12.656441	-10.323649	-5.005847
58 C	6.0000	0	12.011	12.380427	-8.801570	-7.149042
59 C	6.0000	0	12.011	11.692510	-6.250704	-6.952284
60 C	6.0000	0	12.011	11.264109	-5.204740	-4.543506
61 C	6.0000	0	12.011	11.742985	-9.033533	4.269345
62 C	6.0000	0	12.011	12.353196	-11.484206	5.107986
63 C	6.0000	0	12.011	12.961424	-13.340578	3.318359
64 C	6.0000	0	12.011	12.976919	-12.811001	0.728168
65 C	6.0000	0	12.011	12.358393	-12.083476	7.914929
66 C	6.0000	0	12.011	14.187724	2.105760	0.638595
67 C	6.0000	0	12.011	15.161311	4.503520	0.464873
68 C	6.0000	0	12.011	13.640931	6.840242	0.282760
69 C	6.0000	0	12.011	15.451346	8.970927	0.220399
70 C	6.0000	0	12.011	17.943706	8.038800	0.332724
71 C	6.0000	0	12.011	17.849163	5.217345	0.459581
72 O	8.0000	0	15.999	11.296254	7.009259	0.204790
73 C	6.0000	0	12.011	19.931905	3.653219	0.510566
74 C	6.0000	0	12.011	19.766044	0.971508	0.569828
75 N	7.0000	0	14.007	19.636144	-1.232460	0.615654
76 C	6.0000	0	12.011	22.451874	4.584929	0.488532
77 N	7.0000	0	14.007	24.531329	5.324096	0.474491
78 C	6.0000	0	12.011	14.907445	11.526668	0.077233
79 C	6.0000	0	12.011	16.926636	13.230710	0.047432
80 C	6.0000	0	12.011	19.414631	12.337852	0.160665
81 C	6.0000	0	12.011	19.956321	9.750155	0.302564
82 C	6.0000	0	12.011	11.435753	-4.611820	-9.294524
83 C	6.0000	0	12.011	-12.383205	12.138524	-7.841135
84 H	1.0000	0	1.008	-3.511621	-3.872578	0.338431
85 H	1.0000	0	1.008	3.510979	3.876168	-0.349807
86 H	1.0000	0	1.008	-15.548402	-0.582470	-0.826056
87 H	1.0000	0	1.008	-12.958684	-12.149843	-0.076080
88 H	1.0000	0	1.008	-16.572464	-15.243797	-0.037870
89 H	1.0000	0	1.008	-20.966134	-13.672074	-0.224972
90 H	1.0000	0	1.008	-21.898468	-9.130968	-0.441780
91 H	1.0000	0	1.008	-13.442132	3.943613	-3.160850
92 H	1.0000	0	1.008	-14.676388	3.718792	-0.047300
93 H	1.0000	0	1.008	-7.754038	5.578509	-2.743448
94 H	1.0000	0	1.008	-7.079160	5.802688	0.547643
95 H	1.0000	0	1.008	-11.274673	7.626122	-5.604777
96 H	1.0000	0	1.008	-13.424860	15.259255	-3.866115
97 H	1.0000	0	1.008	-13.446951	14.275596	0.710424
98 H	1.0000	0	1.008	-13.185829	12.254666	5.277287
99 H	1.0000	0	1.008	-12.698166	9.540056	9.062673
100 H	1.0000	0	1.008	-10.726709	3.202179	4.382275
101 H	1.0000	0	1.008	-9.584445	3.590669	9.338138
102 H	1.0000	0	1.008	-11.593149	5.667704	11.041141
103 H	1.0000	0	1.008	-12.895510	3.086150	9.346000
104 H	1.0000	0	1.008	13.439638	-3.922694	3.177612
105 H	1.0000	0	1.008	14.675632	-3.718093	0.063419
106 H	1.0000	0	1.008	7.749672	-5.560141	2.764688
107 H	1.0000	0	1.008	7.079783	-5.805069	-0.525949
108 H	1.0000	0	1.008	13.192367	-12.291440	-5.201660
109 H	1.0000	0	1.008	12.705555	-9.604382	-9.006737
110 H	1.0000	0	1.008	10.727333	-3.234115	-4.373204
111 H	1.0000	0	1.008	11.271328	-7.584662	5.645179
112 H	1.0000	0	1.008	13.432721	-15.227659	3.964702
113 H	1.0000	0	1.008	13.457061	-14.277788	-0.619074
114 H	1.0000	0	1.008	12.795600	-14.077288	8.242815
115 H	1.0000	0	1.008	10.510317	-11.679698	8.761451

116	H	1.0000	0	1.008	13.775045	-10.942365	8.908944
117	H	1.0000	0	1.008	15.547722	0.588102	0.818044
118	H	1.0000	0	1.008	12.959213	12.150637	-0.006898
119	H	1.0000	0	1.008	16.573219	15.244062	-0.062512
120	H	1.0000	0	1.008	20.966644	13.673302	0.138215
121	H	1.0000	0	1.008	21.898487	9.133632	0.385353
122	H	1.0000	0	1.008	11.519015	-5.759281	-11.012549
123	H	1.0000	0	1.008	9.637301	-3.584168	-9.286322
124	H	1.0000	0	1.008	12.964617	-3.213555	-9.381073
125	H	1.0000	0	1.008	-12.606798	14.170924	-8.147157
126	H	1.0000	0	1.008	-10.622869	11.535814	-8.751832
127	H	1.0000	0	1.008	-13.952755	11.170625	-8.789721